

Computational discovery of cathode materials for rechargeable aqueous zinc-ion batteries

Caio Miranda Miliante,^{*,†} Brian D. Adams,[‡] Drew Higgins,[¶] and Oleg Rubel[†]

[†]*Department of Materials Science and Engineering, McMaster University, 1280 Main Street West, Hamilton, Ontario L8S 4L8, Canada*

[‡]*Salient Energy Inc., Dartmouth, Nova Scotia B3B 1C4, Canada*

[¶]*Department of Chemical Engineering, McMaster University, 1280 Main Street West, Hamilton, Ontario L8S 4L8, Canada*

E-mail: miliantc@mcmaster.ca

Abstract

Rechargeable aqueous zinc-ion batteries (RAZIBs) attract considerable scientific and commercial interest for deployment in grid-scale energy storage due to higher safety and lower manufacturing cost when compared to lithium-ion batteries. However, currently studied cathode materials suffer from severe capacity fade when cycling at rates appropriate for grid-scale applications (< C/2), which hampers the commercialization of RAZIBs. To address the present limitation on cathode material availability, more than 2000 previously synthesized oxides, chalcogenides, Prussian blue analogues, and polyanion materials were computationally screened for the discovery of highly stable RAZIB cathode materials. The structural, electrochemical, and chemical properties of the materials were respectively evaluated through an investigation of the available Zn^{2+} percolation paths in the crystal structure, the stability of the material in aqueous media under RAZIB operation conditions, and the attained transition

metal oxidation state during cycling. The transition metal oxidation state and intercalating ion coordination environment were determined to govern the magnitude of the calculated intercalation potential, with this finding directly supporting the development of batteries with high operation potentials. Finally, 10 previously unexplored materials (MnBePO_5 , $\alpha\text{-FePO}_4$, $\beta\text{-FePO}_4$, KV_2PO_8 , SrV_2O_6 , $\text{Mo}_2\text{P}_2\text{O}_{11}$, $\text{Cs}_2\text{Mo}_4\text{O}_{13}$, $\text{K}_3\text{Fe}_5(\text{PO}_4)_6$, $\text{CaFe}_3\text{P}_3\text{O}_{13}$, and $\text{SrFe}_3\text{P}_3\text{O}_{13}$) were identified with leading metrics for operation as RAZIB cathode materials, such as high Zn^{2+} (de)intercalation potential, electrochemical stability, theoretical gravimetric capacity, and energy density, being here proposed for experimental testing. The materials identified in this study demonstrate a guide for advancing the available cathode materials for RAZIB, and help expedite the establishment of RAZIB as a commercially viable technology for grid-scale energy storage.

Introduction

Rechargeable batteries have been frequently deployed as grid-scale energy storage infrastructure in support of the energy transition to renewable sources, as batteries have a modular design, smaller footprint, and lower cost.^{1,2} Rechargeable aqueous zinc-ion batteries (RAZIBs), for example, are a promising battery technology for grid-scale applications, being considered significantly safer than potentially flammable lithium-ion batteries (LIBs) due to the use of an aqueous electrolyte.^{3–6} Also, RAZIBs have a lower associated manufacturing cost and utilize a more abundant and non-toxic metal species in Zn, which would allow for an easier scaling from lab to commercial deployment.^{3,5,6} However, currently researched cathode materials for RAZIB suffer from severe capacity fade, especially when cycling at practical rates for grid-scale operation (*i.e.*, C-rates lower than C/2), which directly hampers the RAZIB commercialization efforts.^{3,4,6,7}

Both organic and inorganic materials have already been experimentally investigated as cathode materials for RAZIBs. Organic materials draw considerable interest in the liter-

ature mainly due to their structural diversity, with multiple quinones, imides, imines and conductive polymers already explored.^{4-6,8-12} However, organic materials tend to display lower operation voltages and specific capacities, as well as suffer from structural dissolution into the aqueous electrolyte during cycling, which has severely limited their applicability in RAZIB systems.^{9,11} On the other hand, considerably more promising battery metrics (*i.e.*, specific capacity, operation voltage, and energy density) have been reported for inorganic RAZIB cathode materials, despite the limited variety in structure and composition for the materials explored so far.⁵ Oxides were the first class of materials investigated as cathode materials for RAZIB, as Xu et al.¹³ reported the development of a Zn/ α -MnO₂ battery cell with a mildly acid ZnSO₄ aqueous electrolyte. Since then, MnO₂ polymorphs and other Mn oxides have been extensively explored as cathodes for RAZIB, with the eco-friendly Mn-based cathode cells reporting both high operating potential (ca. 1.5 V vs Zn/Zn²⁺) and discharge capacity (> 200 mA h g⁻¹).^{7,14,15} Current development of oxide materials for RAZIBs is mainly focused Mn- and V-based oxides, with only a few studies reporting the investigation of other transition metal centres (*e.g.*, Mo, Cu) despite the wide range of experimentally realized oxide materials in the literature.^{6,7,16,17}

Polyanionic materials have also been previously investigated as cathode material for RAZIBs, with the scientific interest behind these materials being due to the higher structural stability conferred by the covalent bonds in polyanions.^{6,18} The vast majority of polyanionic cathode materials reported in the literature for RAZIB are phosphorous-based, as silicon- and sulfur-based polyanions have demonstrated poor reversible intercalation within the water stability potential and low electrochemical stability in the aqueous electrolyte.¹⁸ Materials that follow the olivine (*e.g.*, LiFePO₄) and NASICON (sodium super ionic conductor) (*e.g.*, Na₃V₂(PO₄)₃) structural arrangements comprise the majority of polyanions materials investigated as cathodes for RAZIB.¹⁸ However, the development of polyanionic cathode materials is still arguably rooted on structures previously investigated for sodium- and lithium-ion batteries, despite the major difference in electrolyte chemistry being found

in RAZIBs.^{18,19} Polyanions are very attractive as RAZIB cathodes for their high operating potential (up to 1.9 V vs Zn/Zn²⁺), which can be achieved due to the weaker ionic bonding between the metal centre and the oxygen atom induced by, for example, the P-O bonds in phosphates.^{6,18-20} Fluorine is commonly incorporated in polyanions to enhance the inductive effect and increase the RAZIB operating potential, yet its inclusion increases the molecular weight of the active material, which contributes to a lower specific capacity.^{18,19} Chalcogenides and Prussian blue analogue (PBA) have also been previously explored as cathode materials for RAZIB, having displayed reasonable battery operating potentials (> 1.0 V vs Zn/Zn²⁺).^{6,21-23} However, the low specific capacity and/or structural instability of chalcogenides and PBA cathode materials severely hamper their utilization in commercial RAZIB systems.^{6,21,23,24} The stability and specific capacity shortcomings of currently reported cathode materials for RAZIB grants the proposal of novel materials as instrumental in order to fully realize the commercial potential of RAZIBs.

Theoretical calculations have been regularly employed for the discovery and analysis of cathode materials for rechargeable batteries.^{7,15,25-29} Chen et al.³⁰, for example, performed high-throughput screening of novel cathode materials for LIB from density functional theory (DFT) calculations of the material stability, lithium intercalation potential and ion migration barrier. The theoretical results were backed up by the experimental validation of the proposed materials crystal structure and electrochemical performance, resulting in the proposal of carbonophosphates as a novel material class for LIB cathodes.³⁰ Nishijima et al.³¹ systematically investigated cations substitutions in the crystal structure of the well-established LiFePO₄ LIB cathode material in order to extend the battery capacity retention. The Zr and Si substituted material proposed from the theoretical calculations reported an approximately 6 times improvement in number of battery cycles to achieve 80 % capacity retention when compared to the pristine material results.³¹ To date, only a few studies have taken a theory-based approach for the discovery of novel RAZIB cathode materials. Zhou et al.³² trained a machine learning model on the theoretical properties of more than 40,000

inorganic materials available in a database to calculate the respective Zn^{2+} intercalation potential for each material, and proposed almost 10 previously unexplored RAZIB cathode materials. Cai et al.³³ combined high-throughput *ab-initio* calculations of relevant cathode metrics, such as ionic conductivity and volume expansion, and machine learning to screen Zn -containing spinel structures as RAZIB cathode materials. Finally, Wudil et al.³⁴ trained a machine learning model on Zn -containing structures reported on the Materials Project database^{35,36} to predict both the voltage and capacity of novel RAZIB cathode materials.

However, present studies overlook many important aspects during their proposal of novel cathode materials for RAZIB. For example, the electrochemical stability of the materials in aqueous environment is not considered during the screening process, putting into question the stability of the proposed materials for prolonged operation in aqueous media. Many candidate materials also reported battery operation voltages considerably greater than the oxygen evolution reaction (OER) reversible potential, which ultimately would cause the degradation of the aqueous electrolyte employed in RAZIBs. Also, theoretical-only materials (*i.e.*, without previous synthesis) were proposed for experimental testing in RAZIB cells, which casts doubts into the real world application of the reported theoretical framework. Therefore, taking into account the limited amount of theoretical explorations of RAZIB cathode materials reported in the literature and the persistent overlook into critical factors for appropriate cathode performance in present studies, it is possible to identify the currently underdeveloped potential of computational discovery of novel RAZIB cathode materials.

In this study, more than 2000 previously synthesized oxide, chalcogenide, PBA, and polyanion materials available in open databases were screened for the identification of novel cathode materials for RAZIBs. The structural feasibility for Zn^{2+} (de)intercalation was evaluated for each material through the calculation of the available Zn^{2+} percolation paths in the crystal structure. Electrochemically stable materials for continuous operation as cathodes in an aqueous environment were identified through the calculation of the electrochemical decomposition energy in the RAZIB operation potential and pH window from computationally-

obtained Pourbaix diagrams. The redox-active metal centres oxidation states before and after the Zn^{2+} (de)intercalation were also examined with respect to their experimentally determined oxidation states in order to verify the chemical viability of the proposed material operation as a cathode. Overall, 131 materials were identified with having viable crystal structure, electrochemical stability and chemical environment for operation as cathode for RAZIB, for which the Zn^{2+} (de)intercalation potential was calculated through molecular dynamic simulations. The transition metal oxidation state in the cathode material and the Zn^{2+} coordination environment after intercalation were revealed as the main parameters governing the calculated magnitude of Zn^{2+} (de)intercalation potential, which provided significant insight for the development of cathode materials with high battery cycling potentials. Finally, 10 materials (*e.g.*, α -FePO₄, β -FePO₄, MnBePO₅, and SrV₂O₆) were proposed for experimental investigation for the first time due to their higher operation potential, electrochemical stability in aqueous media, gravimetric capacity and/or energy density. The results presented in this work directly support current research efforts towards RAZIB commercialization by proposing multiple experimentally synthesizable next-generation cathode materials with promising battery operation metrics.

Methods

The structures to be explored as potential RAZIB cathode materials were retrieved from the Materials Project database (version 2025.09.25) via its API (application programming interface).^{35,36} Four classes of materials were considered for the investigation based on their previous utilization as RAZIB cathode materials: oxides, chalcogenides, PBAs, and polyanions. The database was queried with respect to the elements considered to be forming the chemical systems of each class. The queried chemical systems for each class are presented in Table 1, with the elements chosen to be investigated being selected based on their toxicity, price and presence in previously explored cathode materials. For example, to get the data

for all Mn-based oxides containing Li available in the database a query equal to ‘Li-Mn-O’ would be utilized. A parenthesis in the chemical systems presented in Table 1 indicates that both systems which include and not include the element inside the parenthesis (or an element of the group inside the parenthesis in the case of *Alk*) were considered during the data retrieval process from the database. Also, the presence or absence of Zn in the structure was considered (‘(Zn)’ in the query) in order to completely explore all potential RAZIB cathode materials available for all classes, be them initially at a charged (*i.e.*, without Zn in the structure) or discharged (*i.e.*, with Zn in the structure) battery state. Only oxide materials containing alkaline and alkaline-earth metals were considered here, since a thorough exploration of binary oxides (corresponding query of ‘*Mtl*-O-(Zn)’) as cathode materials for RAZIB was already performed by our group.⁷ All possible combinations that can be formed from the elements in each query were considered, resulting in 2840 unique chemical systems: 200 for oxides, 660 for chalcogenides, 1100 for PBAs, and 880 for polyanions. In order to guarantee that materials explored in this study can be directly experimentally investigated as RAZIB cathode materials, only structures that were reported by the database as previously synthesized were considered during the query and data retrieval process.

Table 1: Queried systems from the Materials Project database^{35,36} with respect to the elements present in their formulas, where *Alk* indicates an alkali or alkaline earth metal (Li, Na, K, Rb, Cs, Be, Mg, Ca, Sr, or Ba), *Mtl* is a transition metal (Ti, V, Cr, Mn, Fe, Co, Ni, Cu, Mo, or W), and *Chl* is a chalcogen (S, Se, or Te). *Mtl*₁ and *Mtl*₂ are two different transition metal species considered during the query process.

Class	Query
Oxides	<i>Alk</i> - <i>Mtl</i> -O-(Zn)
Chalcogenides	(<i>Alk</i>)- <i>Mtl</i> - <i>Chl</i> -(Zn)
PBAs	(<i>Alk</i>)- <i>Mtl</i> ₁ - <i>Mtl</i> ₂ -C-N-(Zn)
Polyanions	<i>Alk</i> -(F)-(H)- <i>Mtl</i> -O-P-(Zn)

For a material to be a promising RAZIB cathode it is necessary for the material to have sufficient space/voids in its crystal structure for the reversible Zn²⁺ (de)intercalation, which will grant the material higher structural stability during cycling. For this reason, a void search algorithm was coded to parse the crystal structure of all investigated materials and

determine those which have promising structures for cathode operation. The void search algorithm works as follow. First, the crystal lattice parameters and the atomic positions in the lattice are read from the data retrieved from the database for the material in question. Then, an evenly spaced 3D grid is built based on the cell lattice parameters, with the distance between each point in the grid and each atom in the structure (and its periodic images) being then calculated. The smallest distance to an atom in the structure is then determined for each point in the grid, with the distance data being vital in the analysis of the crystal structure, as it allows for the numeric quantification of how vacant (*i.e.*, filled with voids) the structure is depending on the considered distance threshold to an atom in the lattice. For example, Figure 1a shows all the positions inside the α -FePO₄ (mp-19109) lattice which are at least 1.90 Å from an atom in the cell, allowing for the identification of regions in the cell for which Zn²⁺ ions could establish themselves in and bond to the atoms in the host structure after intercalation. A maximum spacing between the 3D grid points of 0.01 Å was chosen for the calculations performed in this study. Also, it is important to note that the chemical nature of the atomic elements are not taken into account when calculating the distance from the grid points to the atoms, therefore, the impact of the atomic radius inside the cell, for example, is not relevant in the void space calculation.

The calculation of the void spaces allows for the determination of the materials with suitable vacancies in their structures for Zn²⁺ intercalation. However, it is important for the intercalating Zn²⁺ ion to have not only space in the structure to establish itself but also an unobstructed path in the structure for it to percolate through during the battery operation. It is then necessary to calculate the available percolation paths, and its complexity, for Zn²⁺ migration in order to determine materials which have promising crystal structure to operate as a RAZIB cathode. For example, if a Zn²⁺ ion migrates to close to other atoms in the structure, the energy barrier associated with the ions movement will be considerably high and consequently deem the ion migration unfeasible to occur. Also, if the percolation path is very elaborate/diverge too much from what would be a straight percolation path, it will

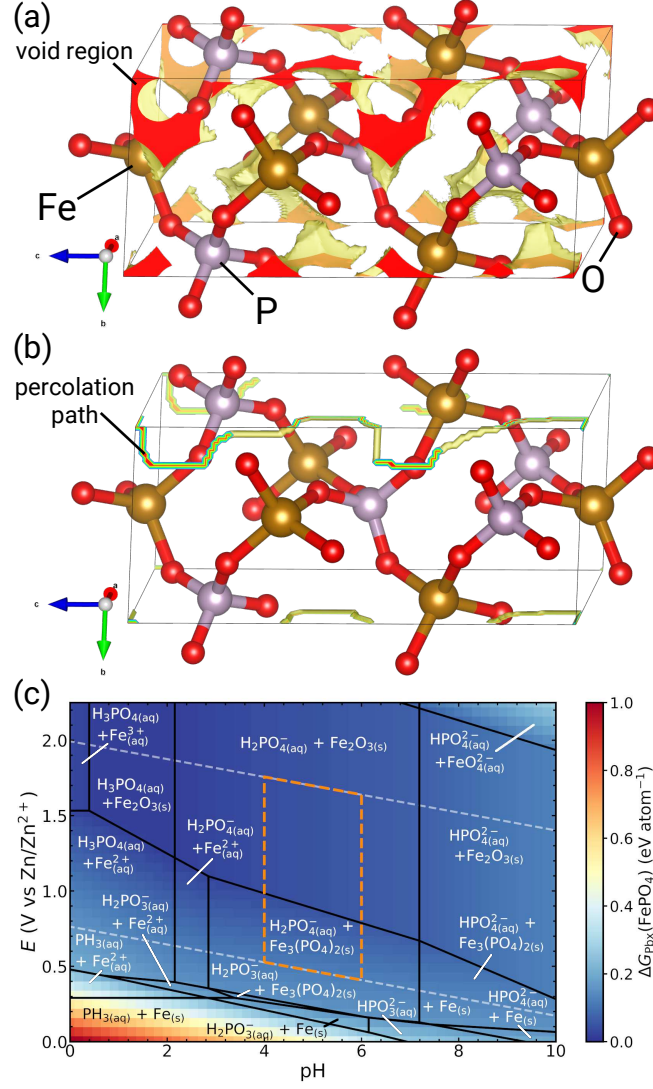


Figure 1: (a) Result for the void search in the α -FePO₄ structure, with the regions in the crystal which are at least 1.90 Å from an atom being presented. (b) Percolation path associated with the maximum percolation path distance ($d_{\text{perc}}^{\text{max}}$) for α -FePO₄, calculated to be equal to 1.87 Å with an associated maximum percolation path deviation (δ_{perc}) of 0.99 Å. (c) Calculated Pourbaix diagram for the Fe-P-H₂O system, alongside a heatmap highlighting the calculated electrochemical decomposition energy (ΔG_{pbx}) for α -FePO₄. The region of interest for RAZIB operation is delimited by the orange dashed lines.

be impractical for the Zn^{2+} to migrate inside the structure. Therefore, to account for an unimpeded Zn^{2+} migration inside the structure and the feasibility of a percolation path, two parameters are introduced here. The first parameter is the percolation path distance (d_{perc}) and it captures the minimum distance that all points along an evaluated percolation path are from an atom in the structure. Materials with higher d_{perc} will then have a more vacant percolation path for Zn^{2+} to migrate through (*i.e.*, unimpeded Zn^{2+} diffusion). The second parameter is the δ_{perc} , which is the maximum distance that a percolation path deviates from being a straight path inside the crystallographic cell. Thus, the closer to 0 Å (value for straight percolation path) the calculated δ_{perc} is the more direct the Zn^{2+} migration within the crystal cell will be.

A percolation path can be calculated based on the 3D grid points established for the void space results, since they already capture the distance to the atoms for all positions inside the lattice, a necessary information for determining d_{perc} . A percolation path can be theoretically considered to start at any point inside the lattice (*e.g.*, $r_i = (0.5, 0.5, 0.5)$ in fractional coordinates), however it is necessary for the path to end at the same lattice point in one of the periodic images (*e.g.*, $r_f = (1.5, 0.5, 0.5)$). This requirement guarantees that the entire structure would be crossed by the percolating ion if it followed the calculated path, as it would return to a position crystallographically identical to its starting point. In the algorithm established here for the calculation of the percolation path, first, a high initial d_{perc} guess value is chosen (15 Å was used here). Then, the shortest path that can be established by connecting adjacent grid points that are at least d_{perc} from an atom in the structure is calculated, taking into account the discussed requirement for the start and end point. If the percolation path could not be established, then the evaluated d_{perc} is decreased by a small factor (0.01 Å was used here) and the percolation path search is restarted. However, if a percolation path is found, then a viable d_{perc} value for the structure was found. The d_{perc} found through this method is also then called the $d_{\text{perc}}^{\text{max}}$, since it is the highest distance for which a percolation path can be established inside the crystal cell. For any distance of less

than $d_{\text{perc}}^{\text{max}}$ it will be possible to establish a percolation path inside the structure, with these distinct percolation paths also having different d_{perc} and δ_{perc} values associated with them. The percolation path for $\alpha\text{-FePO}_4$ with a $d_{\text{perc}}^{\text{max}}$ equal to 1.87 Å and an associated δ_{perc} of 0.99 Å is shown as an example in Figure 1b.

The utilization of aqueous electrolytes in RAZIB adds further stability considerations when evaluating the proposal of novel cathode materials, as active material dissolution into the electrolyte has been shown to occur in both organic and inorganic RAZIB cathode materials during cycling.^{9,24,37} The electrochemical stability in an aqueous environment at RAZIB operation conditions was evaluated through an analysis of computationally-obtained Pourbaix diagrams, an approach which has already been shown to appropriately capture the stability limitation of cathode materials in aqueous batteries.^{7,15,38} The diagrams for the electrochemical stability analysis were constructed with the use of the Materials Project Pourbaix diagram tool,^{39–41} which reports the electrochemical decomposition energy (ΔG_{pbx}) for a material at different applied potentials and pH conditions evaluated during diagram construction. The ΔG_{pbx} shows how unstable an investigated material is with respect to the thermodynamically stable material at potential and pH condition of interest. For this reason, materials with lower ΔG_{pbx} values can be considered to be more electrochemically stable for use as a RAZIB cathode material. The conditions of interest for the electrochemical stability analysis were of an electrode potential (E) between the reversible potentials for the hydrogen evolution reaction (HER) and oxygen evolution reaction (OER), to avoid the degradation of the aqueous electrolyte, and pH levels between 4 and 6, considering previous reports on electrolyte pH fluctuation during RAZIB operation.^{38,42} The average electrochemical decomposition energy ($\langle \Delta G_{\text{pbx}} \rangle$) is then calculated with respect to the ΔG_{pbx} values reported within the E -pH operation window to quantify the electrochemical instability of the materials in the condition of interest for RAZIB cathode operation. The calculated Pourbaix diagram for $\alpha\text{-FePO}_4$ ($\langle \Delta G_{\text{pbx}} \rangle = 0.06 \text{ eV atom}^{-1}$) is presented on Figure 1c as an example, with a heatmap displaying the calculated ΔG_{pbx} values for the material at the different E

and pH conditions.

The transition metal atoms undergo a redox reaction during the Zn^{2+} (de)intercalation process. Therefore, it is important to verify that the oxidation states attained by the metal centres after the (de)intercalation continue to be chemically feasible. The experimentally observed oxidation states for all transition metals considered in this study were first compiled, with the theoretical metal centres oxidation states in each material prior to (de)intercalation also calculated. For materials that are retrieved from the database at a expected charged battery state (*i.e.*, without Zn in the structure), if the metal centre in the structure was already at the lowest experimental oxidation state for that specie, the material was then considered invalid for use as a cathode material. The material disqualification is due to the chemical inaccuracy that would be achieved, since the evaluated metal centre would be predicted to reduce to an oxidation state lower than what has been experimentally verified after Zn^{2+} ion intercalate into the structure. Conversely, for materials that are reported to be at a discharged state (*i.e.*, materials with Zn in the structure), the structure is considered invalid for use as cathode if the metal centre already is on its highest oxidation state prior to Zn^{2+} deintercalation . All other oxidation states for the transition metals were considered as valid.

It is then necessary to determine if the Zn^{2+} (de)intercalation process is thermodynamically feasible to occur in the studied structures to validate their application as cathodes for RAZIB. The energetic feasibility for Zn^{2+} (de)intercalation can be probed by calculating the Zn^{2+} (de)intercalation energy (ΔH_{Zn}) (in eV)

$$\Delta H_{Zn} = U_{\text{tot}}(M_{\text{dchg}}) - U_{\text{tot}}(M_{\text{chg}}) - z u_{\text{tot}}(Zn_{\text{bulk}}), \quad (1)$$

where $U_{\text{tot}}(i)$ is the total energy (in eV) calculated for system i , M_{dchg} and M_{chg} are the studied materials at a discharge and charged battery state, respectively, z is the number of Zn atoms that (de)intercalated, $u_{\text{tot}}(i)$ is the total energy per atom (in eV atom $^{-1}$) calculated

for system i , and Zn_{bulk} is the bulk structure of Zn. A negative ΔH_{Zn} value indicate that the Zn^{2+} (de)intercalation process is energetically viable to occur in the structure, while positive values indicate that the process is energetically unpractical to occur. The Zn^{2+} (de)intercalation potential (E_{Zn}) (in V vs. Zn/Zn^{2+}) can then be calculated based on the Nerst equation

$$E_{\text{Zn}} = -\frac{\Delta H_{\text{Zn}}}{n_e e}, \quad (2)$$

where n_e is the number of electrons transferred in the Zn^{2+} (de)intercalation process and e is the elementary charge.

The structure total energy were calculated from molecular dynamics (MD) simulations ran with the MACE mp-0 interatomic potential,^{43,44} which has been parametrized with respect on the DFT data available on the Materials Project database.^{35,36} The molecular dynamics simulations were run for 50 ps with a 1 fs timestep under a NPT ensemble following the methodology proposed by Melchionna et al.^{45,46} Constant Nosé-Hoover thermostat ($ttime = 25$ fs) and Parinello-Rahman barostat ($pfactor = 10^6$ GPa fs²) respectively set to 300 K and 1 bar were employed, with all MD simulations being run utilizing the atomic simulation environment (ASE) Python library.⁴⁷ To create the M_{dchg} and M_{chg} supercells to be simulated, the initial crystallographic cells obtained from the Materials Project database were replicated in all 3 dimension so at least 100 atoms were present in the supercells. If the phase extracted from the database already contained Zn in its structure (M_{dchg} - *e.g.*, SrV_2ZnO_7 , $NaVZnP_2O_9$), the M_{chg} phase was created by removing a random Zn atom present in the M_{dchg} supercell (*i.e.*, Zn^{2+} deintercalation process). However, if the material obtained from the database did not contain Zn (M_{chg} - *e.g.*, $LiMoP_2O_7$, $K_2Ti_6O_{13}$), the initial M_{dchg} phase was then created by placing a Zn atom on the position most distant from other atoms on the calculated $d_{\text{perc}}^{\text{max}}$ percolation path for the associated M_{chg} structure (*i.e.*, Zn^{2+} intercalation process). In both cases, the E_{Zn} is calculated with respect to a single Zn^{2+} ion deintercalating or intercalating into the structure, directly indicating the expected potential to be obtained from the utilization of the respective materials as cathodes for RAZIBs. A

value of z of 1 and n_e of 2 was then considered for all ΔH_{Zn} and E_{Zn} calculations (see Eqs. (1) and (2)), since there was only one double charged Zn^{2+} ion of difference between the atomic compositions of the M_{dchg} and M_{chg} structures.

Relevant metrics for RAZIB operation, such as theoretical gravimetric capacity (Q_w) and theoretical energy density (W_w), were calculated for the proposed materials for experimental investigation. The Q_w (in mA h g^{-1}) for a cathode material can be calculated from

$$Q_w = \frac{\eta F}{3.6W}, \quad (3)$$

where η is the number of electrons considered in the battery discharge reaction per cathode formula, F is the Faraday constant ($96,485 \text{ C mol}^{-1}$), and W is the molecular weight of the cathode material at its charged state (in g mol^{-1}). The variation of only a single metallic centre oxidation state was considered here for the calculation of Q_w (*e.g.*, Mtl^{3+} to Mtl^{2+}), thus η was equal to 1 for all materials. The W_w (in W h kg^{-1}) can then be directly calculated from the E_{Zn} and Q_w results

$$W_w = Q_w E_{\text{Zn}}. \quad (4)$$

The magnitude of Mtl-O bonding strength was calculated for selected materials via the computation of the projected crystal orbital Hamilton population (pCOHP) utilizing the LOBSTER package.^{48–51} Density functional theory (DFT) calculations with projector augmented wave pseudopotentials⁵² (14, 5, and 6 valency electrons considered for Fe, P, and O, respectively) were carried out for performing the pCOHP analysis, utilizing the Perdew-Burke-Ernzerhof exchange-correlational functional⁵³ as implemented in VASP^{54–56} (version 6.4.3). A plane-wave cutoff energy of 520 eV was utilized in all calculations, with the DFT-D3 method with Becke-Johnson damping function employed to account for the van der Waals interactions in the materials.^{57–61} Initial ferromagnetic ordering for spin-polarized calculations was employed for all materials, following the reported magnetism for the investigated materials from the database.^{35,36} Hubbard U correction was considered for the d electrons of

Fe ($U_{\text{eff}} = 5.3$ eV^{35,62}).⁶³ A Γ -centred k -point grid of $6 \times 4 \times 2$ and $6 \times 6 \times 3$ were respectively employed for the calculations for *olivine*-FePO₄ (mp-20361) and α -FePO₄ (mp-19109). The structures obtained from the database were submitted to cell and atomic position relaxation before calculation of the pCOHP, with convergency tolerances of 10^{-7} eV and 10^{-1} eV Å⁻¹ respectively considered for the energy change in consecutive self-consistent loops and for the norm of ionic forces.

The code written for this project (void search, percolation path and electrochemical stability analysis) was programmed in Python, and is available online.

Results and discussion

In total, the data for 2046 previously synthesized materials were extracted from the database based on the queried chemical systems, with 720 materials being from the oxide class, 509 chalcogenides, 27 PBAs, and 790 polyanions. Fe (365 materials), V (305 materials) and Mn (246 materials) were the transition metals with the highest frequency in the materials obtained from the database, comprising together approximately 45 % of all materials investigated. The identification of numerous V- and Mn-based materials during the query process is favourable for the identification of novel RAZIB cathode materials, since multiple materials containing these metal centres have been demonstrated to be electrochemically active as cathodes for RAZIBs.^{6,18,19} A summary of all materials reported from the database with respect to their classes and transition metal centres is shown in Figure S1.

The feasibility for Zn²⁺ migration through the structure and the electrochemical stability of the host material were respectively evaluated with the calculation of maximum percolation path distance ($d_{\text{perc}}^{\text{max}}$) and average electrochemical decomposition energy ($\langle \Delta G_{\text{pbx}} \rangle$) (see Methods section). The results for $d_{\text{perc}}^{\text{max}}$ and $\langle \Delta G_{\text{pbx}} \rangle$ for all considered materials can be seen in Figure 2a, with the results separated per material class being shown in Figure S2. First, the electrochemical stability of the queried materials will be investigated. From the

$\langle \Delta G_{\text{pbx}} \rangle$ results, a clear relationship between electrochemical stability and material class was able to be identified. Oxides and polyanions are concentrated at lower $\langle \Delta G_{\text{pbx}} \rangle$ values, with only a few materials from these classes reporting $\langle \Delta G_{\text{pbx}} \rangle$ greater than 1 eV atom⁻¹ (Fig. 2a and S2). On the other hand, chalcogenides and PBAs reported higher $\langle \Delta G_{\text{pbx}} \rangle$, with a considerable range of $\langle \Delta G_{\text{pbx}} \rangle$ results being captured for chalcogenides (approximately from 0.5 to 3.3 eV atom⁻¹). The electrochemical stability of each class was then individually investigated in order to understand the relationship between material class and $\langle \Delta G_{\text{pbx}} \rangle$ for the proposal of novel RAZIB cathodes.

To understand the wide range of results for the electrochemical stability of chalcogenides, the calculated $\langle \Delta G_{\text{pbx}} \rangle$ values for the class were plotted with respect to the individual chalcogen atom present in the materials (*i.e.*, S, Se, or Te), as shown in Figure S3. It is possible to attest that there is a clear relationship between $\langle \Delta G_{\text{pbx}} \rangle$ and chalcogen atom centre, with Se-containing materials being more electrochemically stable, followed by materials with Te and then S. This trend between chalcogen element and calculated $\langle \Delta G_{\text{pbx}} \rangle$ can be explained from the electrochemical stability of each element in aqueous solutions as captured by their individual experimentally-obtained Pourbaix diagram.⁶⁴ In the conditions of interest for RAZIBs (*i.e.*, $E(\text{HER}) < E_{\text{Zn}} < E(\text{OER})$ and $4 < \text{pH} < 6$, see Methods section), S is thermodynamically favoured to form an aqueous species SO_4^{2-} _(aq), with solid phases, such as $\text{S}_{(\text{s})}$ and $\text{H}_2\text{S}_{(\text{s})}$, only being established at potentials close to HER.⁶⁵ On the other hand, solid phases of Te ($\text{Te}_{(\text{s})}$, $\text{TeO}_2{}_{(\text{s})}$ ⁶⁶), and especially Se ($\text{Se}_{(\text{s})}$ ⁶⁷), were observed to be formed at a wide potential and pH range within the conditions of interest for RAZIBs. The prevalence for the formation of solid Se and Te phases from the analysis of their Pourbaix diagram points to an overall higher electrochemical stability (lower $\langle \Delta G_{\text{pbx}} \rangle$) for solid materials containing these chalcogen elements than those which contain S. However, despite the lower $\langle \Delta G_{\text{pbx}} \rangle$ results found for chalcogenides containing Se and Te, chalcogenides materials were still considered to be highly unstable in aqueous media (high $\langle \Delta G_{\text{pbx}} \rangle$), which will cause for chalcogenides to be more prone to degradation and capacity fade when operating

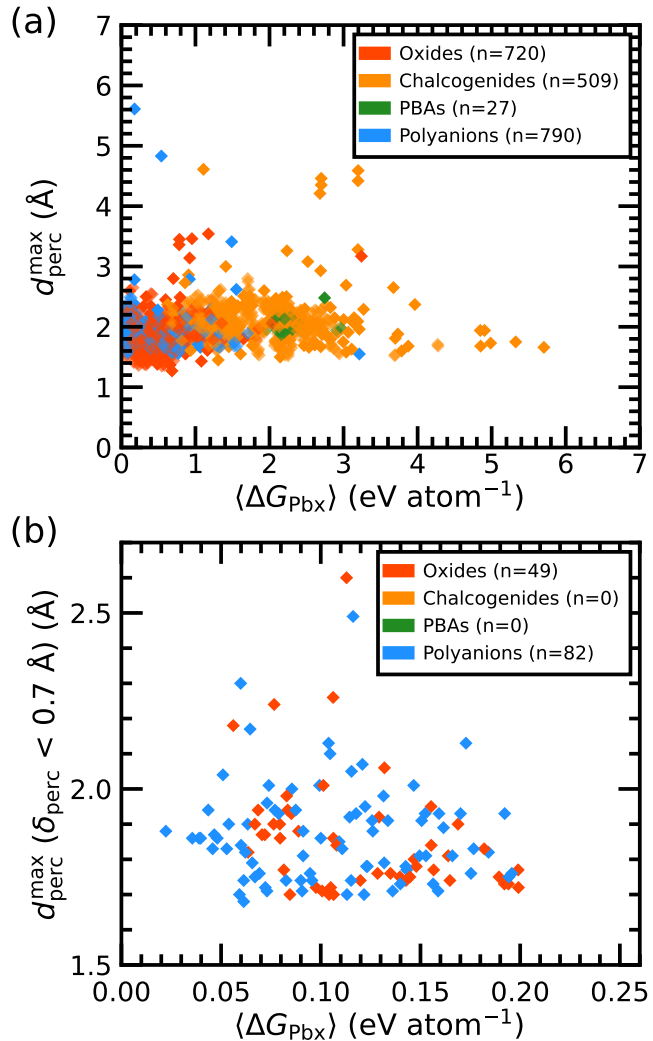


Figure 2: (a) Maximum percolation path distance (d_{perc}^{\max}) as a function of the average electrochemical decomposition energy ($\langle \Delta G_{\text{pbx}} \rangle$) for all materials considered. (b) d_{perc}^{\max} for a maximum percolation path deviation (δ_{perc}) of less than 0.7 Å ($d_{\text{perc}}^{\max}(\delta_{\text{perc}} < 0.7 \text{\AA})$) and $\langle \Delta G_{\text{pbx}} \rangle$ results for materials considered for E_{Zn} calculation.

as cathode materials for RAZIBs. This conclusion is in agreement with previous reports on bulk chalcogenide materials as RAZIB cathodes, in which modifications to the chalcogenide structure were necessary to be implemented in order to achieve reasonable capacity retention at practical current densities for grid-scale application.⁶⁸

The PBA materials investigated also reported high $\langle \Delta G_{\text{pbx}} \rangle$ values, with the results concentrated around 2 eV atom⁻¹ indicating an overall low electrochemical stability for PBAs as RAZIB cathodes. The $\langle \Delta G_{\text{pbx}} \rangle$ results for the PBAs can also be explained from the investigation of the Pourbaix diagrams of the constituting elements, similarly to how was done for the $\langle \Delta G_{\text{pbx}} \rangle$ in chalcogenides. From the Pourbaix diagrams of C and N it is possible to see that the formation of aqueous dissolved species is favoured in the RAZIB conditions of interest for both elements ($\text{H}_2\text{CO}_{3(\text{aq})}$ for C,⁶⁹ and $\text{NH}_{4(\text{aq})}^+$ and $\text{NO}_{3(\text{aq})}^-$ for N⁷⁰). The presence of dissolved species of C and N would then explain the instability of PBAs in aqueous environments as captured by the high $\langle \Delta G_{\text{pbx}} \rangle$ results captured for the class. However, it is important to note that only 27 experimentally obtained materials with PBAs chemistry were able to be identified from the database, which ultimately limits the conclusions shown here with respect to the electrochemical stability of PBA cathodes. In order to screen for materials with high electrochemical stability as cathodes for RAZIBs, only materials with calculated $\langle \Delta G_{\text{pbx}} \rangle$ lower or equal to 0.2 eV atom⁻¹ continued to be considered during the screening process. The electrochemical stability criteria considerably reduced the number of candidate materials from 2046 to 678, as shown in Figure 3. 502 of the remaining materials were polyanions and 176 oxides, with all the chalcogenides and PBAs being filtered out, as can be expected from the $\langle \Delta G_{\text{pbx}} \rangle$ discussion.

For screening the Zn^{2+} migration path, it is important to note that materials with very high or low d_{perc} would not allow for appropriate Zn^{2+} intercalation in the host structure, since the ion would not be able to establish bonds with suitable lengths. Also, as discussed previously on the Methods section, the calculated percolation path distance (d_{perc}) is also dependent on the δ_{perc} , which accounts for how linear (or not) a given percolation path

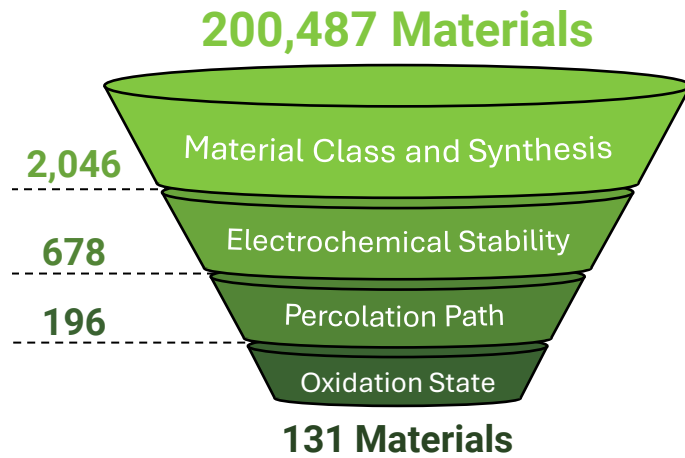


Figure 3: Parameters utilized for the screening of novel RAZIB cathode materials, with number of remaining candidate materials after each screening parameter also presented.

is. The more linear a percolation path is, the easier it can be expected for the Zn^{2+} to transverse through the given path, since there is a more direct path for Zn^{2+} intercalation in the material. The effect of δ_{perc} on the feasibility for Zn^{2+} ion migration can be attested by comparing the paths for materials with the same calculated d_{perc}^{\max} , but different δ_{perc} . For example, a d_{perc}^{\max} of 1.75 Å was calculated for both Li_3VO_4 (mp-19219) and $Sr_2V_2O_7$ (mp-19660), with their respective paths being shown in Figure S4. The percolation path found for Li_3VO_4 is straight ($\delta_{perc} = 0.00$ Å) throughout the crystal cell (see Figure S4a,b), which will cause for the ion migration to be less challenging, while a more obstructed migration will be found in $Sr_2V_2O_7$ ($\delta_{perc} = 4.74$ Å) due to the complex percolation path (see Figure S4c,d). Therefore, it is necessary to take into consideration both d_{perc}^{\max} and δ_{perc} when screening for potential materials to be employed as RAZIB cathodes. For this reason, the d_{perc}^{\max} for each material at different maximum δ_{perc} values were also calculated, allowing for a more precise comparison of d_{perc}^{\max} values between materials, since all parameters would be under the same displacement criteria.

To determine the d_{perc}^{\max} and δ_{perc} parameters to be considered in the screening process, the percolation path in commonly employed cathode materials for RAZIB was calculated.⁵ The materials selected were: α - MnO_2 (mp-19395) ($d_{perc}^{\max} = 2.48$ Å with $\delta_{perc} = 0.00$ Å), β - MnO_2

(mp-510408) ($d_{\text{perc}}^{\text{max}} = 1.60 \text{ \AA}$ with $\delta_{\text{perc}} = 0.62 \text{ \AA}$), V_2O_5 (mp-510408) ($d_{\text{perc}}^{\text{max}} = 2.34 \text{ \AA}$ with $\delta_{\text{perc}} = 0.00 \text{ \AA}$), $\text{VO}_2(\text{B})$ (mp-541404) ($d_{\text{perc}}^{\text{max}} = 1.75 \text{ \AA}$ with $\delta_{\text{perc}} = 1.13 \text{ \AA}$). From the obtained results from previously studied RAZIB cathodes, a δ_{perc} limit of 0.7 \AA was then chosen as the maximum displacement for which the $d_{\text{perc}}^{\text{max}}$ would be analyzed for, as the δ_{perc} cap would still allow for realistic percolation paths to be established inside the host structures. The criteria for the evaluation of the Zn^{2+} migration path was then established to be of a $d_{\text{perc}}^{\text{max}}$ between 1.7 \AA and 2.5 \AA for a δ_{perc} of less than 0.7 \AA ($d_{\text{perc}}^{\text{max}}(\delta_{\text{perc}} < 0.7 \text{ \AA})$). The number of remaining viable candidates was then reduced to 196 materials (see Fig. 3), with only materials that did not already have Zn atoms in the structure being considered during the Zn^{2+} percolation path screening process.

It is important to note that it is common in the literature to evaluate the migration of a intercalating ion in battery cathode materials through the calculation of the migration energy barrier using, for example, the nudged elastic band (NEB) method.^{71,72} Such calculations are able to provide valuable insight into the cathode material by mapping the minimum energy path for ionic migration in the structure and the associated energetic barrier.⁷¹ However, the computational expense associated with accurately capturing the optimal path for ion migration, and its associated energy barrier, is considerably high, since individual DFT calculations are necessary for each ionic position image in the studied migration path. The computational cost for migration energy barrier calculation made it unfeasible for such calculations to be implemented in this study, given the elevated number of materials being investigated. Therefore, a faster and computationally cheaper method for the identification of feasible structures for Zn^{2+} migration based on the available percolation path was implemented. The established $d_{\text{perc}}^{\text{max}}$ and δ_{perc} criteria for percolation path screening are expected to capture structures with low migration energy barriers, since the selected materials will then have a direct and spacious path for unobstructed Zn^{2+} migration available in its structure.

Finally, the oxidation states of the transition metal centres in the remaining candidates were investigated to determine the materials that were indeed chemically feasible for oper-

ation as a cathode. 131 materials were concluded to be viable candidate RAZIB cathode material due to their combined high electrochemical stability, availability for Zn^{2+} migration path and practical metallic centre redox couple (see Fig. 3). From the 131 materials selected for E_{Zn} calculation, 82 of them were polyanions and 49 were oxides, with the majority of the materials having V (47) or Mo (23) as their metal centres (see Fig. S5). Figure 2b shows the distribution of the selected materials for E_{Zn} calculation with respect to $\langle \Delta G_{pbx} \rangle$ and $d_{perc}^{\max}(\delta_{perc} < 0.7 \text{ \AA})$. The calculated $d_{perc}^{\max}(\delta_{perc} < 0.7 \text{ \AA})$ for PWO_5 (mp-554866) ($d_{perc}^{\max}(\delta_{perc} < 0.7 \text{ \AA}) = 2.78 \text{ \AA}$) was higher than the screening limit 2.5 \AA (see Figure 2b). However, PWO_5 was still considered for E_{Zn} calculation, since it was determined that a percolation path with lower δ_{perc} than 0.7 \AA is able to be established in the structure and also be within the d_{perc} screening range ($1.7 \text{ \AA} < d_{perc} < 2.5 \text{ \AA}$). The data compiled for all materials used in the analysis of the electrochemical stability, Zn^{2+} ion percolation path, and chemical feasibility for cathode operation is available online, allowing other researchers to implement different screening parameters limits for the exploration of novel RAZIB cathodes.

The E_{Zn} calculated for all remaining candidate materials is presented in Figure 4. First, the literature was queried to identify which of the screened materials had been previously experimentally investigated as cathode for RAZIBs to validate the E_{Zn} prediction capability. In total, 5 materials (3 oxides and 2 polyanions) were found to have had previous experimental reports, with these materials being highlighted in Figure 4 with an outer black line on their markers. The experimental intercalation potential for these materials are presented in Table 2, alongside the theoretical results calculated in this study. Overall, strong agreement can be seen between the experimental and theoretical Zn^{2+} intercalation potential results, with absolute errors of less than 0.2 V being seen for all materials. The agreement between the theoretical and experimental results, independently of the class, validates the predictive capability of the methodology employed in this study for the calculation of E_{Zn} . The agreement also allows for a more substantiated analysis of the calculated E_{Zn} results for the previously unexplored results and the proposal of novel materials for experimental

investigation as RAZIB cathodes.

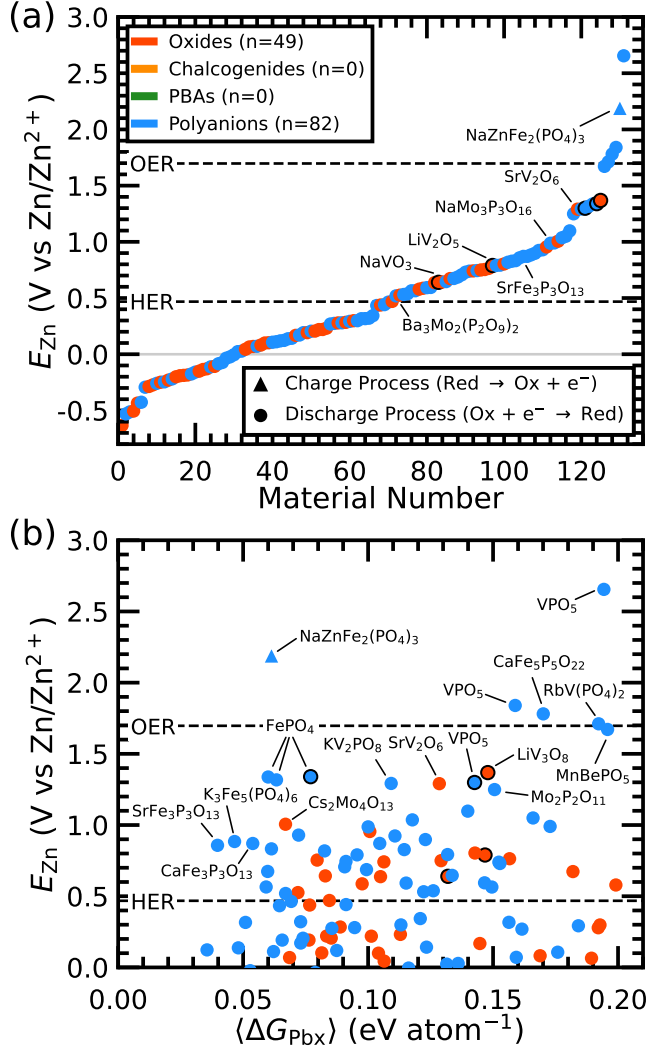


Figure 4: Calculated Zn^{2+} (de)intercalation potential (E_{Zn}) results for all materials plotted (a) in the order of increasing potential and (b) with respect to the material average electrochemical decomposition energy ($\langle \Delta G_{\text{pbx}} \rangle$). Materials that have been previously experimentally investigated are highlighted in the graphs with an outer black line on their markers. The dashed lines represent the HER and OER reversible potentials calculated at a pH = 5 and $[\text{Zn}^{2+}] = 1 \text{ M}$.

For the Zn^{2+} (de)intercalation in a cathode material to be energetically favourable it is necessary for Zn^{2+} (de)intercalation energy (ΔH_{Zn}) to be negative, which would then lead to positive Zn^{2+} (de)intercalation potential (E_{Zn}) values (see Eqs. (1) and (2)). However, 30 of the investigated materials reported positive ΔH_{Zn} values, indicating that Zn^{2+} would not intercalate into the materials at feasible potentials for operation as cathodes for RAZIB.

Table 2: Experimental and theoretical (this work) Zn^{2+} intercalation potential results for screened materials that have already been experimentally investigated. Experimental results are approximate and will reflect the expected potential associated with the initial Zn^{2+} intercalation.

Material	Zn^{2+} Intercalation Potential (V vs Zn/Zn^{2+})	
	Experimental	Theoretical
LiV_3O_8 (mp-27503)	$1.3^{73,74}$	1.37
<i>olivine</i> - $FePO_4$ (mp-20361)	1.2^{75}	1.34
VPO_5 (mp-554181)	1.5^{76}	1.30
LiV_2O_5 (mp-19408)	0.9^{77}	0.79
$NaVO_3$ (mp-555665)	0.8^{78}	0.64

These materials can be identified in Figure 4a by having their reported potentials being less than 0 V vs Zn/Zn^{2+} . Also, other 40 materials reported positive E_{Zn} that were less than the reversible potential for HER, while E_{Zn} greater than the reversible potential for the OER was found for 5 materials. By not reporting E_{Zn} within the range for stable electrolyte operation (*i.e.*, $E(\text{HER}) < E_{Zn} < E(\text{OER})$), all 45 materials would be theoretically unfeasible for operation as RAZIB cathode due to the risk of electrolyte degradation at the predicted battery cycling potentials. To understand why more than half of the materials investigated reported E_{Zn} unfeasible for application as a RAZIB cathode, the metal centres oxidation state and the chemical environment for Zn^{2+} (de)intercalation were investigated.

It has long been established in the LIB literature the direct relationship between higher metallic centre oxidation state and higher battery operation potentials for redox couples with the same crystal structure (*i.e.*, $E(Mtl^{4+}/Mtl^{3+})$ will be greater than $E(Mtl^{3+}/Mtl^{2+})$ for the same Mtl species).^{79,80} The direct relationship between metallic oxidation state and intercalation potential was also demonstrated by our group on the investigation of binary oxides as cathodes for RAZIBs.⁷ When evaluating the E_{Zn} results for the polyanions and oxide materials investigated here, a similar trend between oxidation state and Zn^{2+} (de)intercalation potential was observed, as shown in Figure S6. The trend can be clearly seen for metals which had the E_{Zn} calculated for materials at varied oxidation states, such as V and Mo. The results show that materials with high average oxidation states (*e.g.*, V^{5+} in LiV_3O_8

(mp-27503) and KV_2PO_8 (mp-557947), and $\text{Mo}^{5.33+}$ in $\text{LiMo}_3\text{P}_3\text{O}_{16}$ (mp-17314)) reported potentials greater than 1 V vs Zn/Zn^{2+} while materials with lower average oxidation states (*e.g.*, V^{3+} in KVP_2O_7 (mp-16812), and Mo^{3+} in LiMoP_2O_7 (mp-18987)) tend to return lower and even negative E_{Zn} values (see Fig. S6). Also, metallic redox couples previously identified as being impractical for RAZIB cathode application due to their low Zn^{2+} intercalation potential⁷ (*e.g.*, metal oxidation state at charged battery state (M_{chg}) equal to Ti^{4+} , V^{3+} , Cr^{3+} , Mo^{3+} , or W^{5+}) were also identified here as having negligible E_{Zn} .

However, the calculated E_{Zn} results can not be explained solely from the metal centres oxidation states, as some materials do not follow the expected trend. For example, RbVPHO_6 (mp-1201601) (V^{5+} , 0.12 V vs Zn/Zn^{2+}), Rb_2MoO_4 (mp-19212) (Mo^{6+} , -0.29 V vs Zn/Zn^{2+}), and Li_3VO_4 (mp-19219) (V^{5+} , 0.06 V vs Zn/Zn^{2+}) have high average metallic oxidation state, but return very low E_{Zn} . In order to explain why these and other materials do not follow the expected metallic oxidation state trend, and also why the calculated E_{Zn} results are scattered through a wide potential range (see Figure 4), it is necessary to look into the chemical environments established after Zn^{2+} intercalation. Zn atoms are preferably bonded in inorganic structures through a tetrahedral or octahedral coordination, as a result of the complete filling of the degenerate molecular orbitals by the Zn^{2+} d^{10} electrons.⁸¹⁻⁸⁴ When investigating the Zn^{2+} bonding in the materials which did not follow the oxidation state trend, it is possible to attest that the coordination environments established after the MD relaxation are not energetically favourable. For example, the intercalated Zn^{2+} ion is bonded to RbVPHO_6 through a planar coordination (Fig. S7a,b), while angular and distorted tetrahedral coordinations were found for Rb_2MoO_4 (Fig. S7c,d) and Li_3VO_4 (Fig. S7e,f), respectively. On the other hand, structures which reported high E_{Zn} , and followed the expected trend with respect to the metallic oxidation state, had the intercalated Zn^{2+} atom in an energetically favourable coordination environment. For example, the energetically favourable tetrahedral coordination was established in the relaxed structures of KV_2PO_8 (mp-557947) (V^{5+} , 1.30 V vs Zn/Zn^{2+}) (Fig. S8a,b), $\text{Cs}_2\text{Mo}_4\text{O}_{13}$ (mp-1202511) (Mo^{6+} , 1.00 V vs Zn/Zn^{2+})

(Fig. S8c,d), BaV_2O_6 (mp-18929) (V^{5+} , 0.95 V vs Zn/Zn^{2+}) (Fig. S8e,f), demonstrating a direct relationship between high E_{Zn} and favourable Zn^{2+} coordination environment in the structure. However, the consideration of suitable Zn^{2+} coordination environment is often overlooked during the investigation of novel cathode materials, with researchers proposing materials with considerably large interlayer spacing and tunnels which will not necessarily support stable Zn^{2+} intercalation.^{85,86} From the analysis of the E_{Zn} results for the investigated materials, it is possible to conclude that to realize RAZIBs with high Zn^{2+} intercalation potential it is important to screen for novel cathode materials that have redox active species at high oxidation states, and also a crystal structure that allow for the establishment of energetically favourable Zn^{2+} coordinations after intercalation. It is important to note that the considerations presented here (*i.e.*, high oxidation state for the redox active species, and favourable structural environment for forming stable ion intercalation) are also applicable for the discovery of novel cathode materials with high operation potentials in other intercalating ion battery chemistries, since the conclusions obtained from the E_{Zn} analysis are independent of the investigated RAZIB chemistry. For other intercalating ions (*e.g.*, Na^+ , Ca^{2+}), the energetically favourable ion coordination environment will not necessarily be the tetrahedral and octahedral coordination environments established for Zn^{2+} .

In total, 56 materials were found to have suitable electrochemical stability, structural availability for Zn^{2+} percolation, chemically reasonable transition metal oxidation state and Zn^{2+} (de)intercalation potential (*i.e.*, $E(\text{HER}) < E_{\text{Zn}} < E(\text{OER})$) for use as a cathode in RAZIBs. As presented in Table 2, 5 out of the 56 materials identified have already being previously explored as RAZIB cathodes, but no reports were found for the remaining materials. The majority of the newly identified materials (33 out of 51) report considerably low E_{Zn} (lower than 0.85 V vs Zn/Zn^{2+}), deeming them of low scientific interest as RAZIB cathodes. However, the remaining 18 materials display significant E_{Zn} and high electrochemical stability, which warrants a deeper investigation as potential next-generation RAZIB cathode materials. The list of materials identified in this study being recommended

for further experimental testing is presented on Table 3. The leading materials being here proposed are two polymorphs of FePO_4 , α - FePO_4 and β - FePO_4 , due to their elevated predicted operation potential ($E_{\text{Zn}} > 1.3$ V vs Zn/Zn^{2+}) and high electrochemical stability ($\langle\Delta G_{\text{pbx}}\rangle = 0.06$ eV atom $^{-1}$). Both materials also reported two of the highest theoretical gravimetric capacity (Q_{w}) (> 170 mA h g $^{-1}$) and theoretical energy density (W_{w}) (> 230 W h kg $^{-1}$) metrics from all of the screened materials with relevant E_{Zn} for RAZIB application, with Q_{w} and W_{w} being crucial figures of merit for energy storage applications. The proposal of the α and β polymorphs of FePO_4 for experimental testing as RAZIB cathodes is further supported by previous reports of RAZIB cycling utilizing an *olivine* polymorph and an amorphous phase of FePO_4 as RAZIB cathodes.^{75,87} MnBePO_5 , KV_2PO_8 , SrV_2O_6 , and $\text{Mo}_2\text{P}_2\text{O}_{11}$ also reported considerably high Zn^{2+} intercalation potentials, theoretical capacities, and theoretical energy densities, which also positions these materials as promising candidate cathode materials. However, the noticeably higher electrochemical instability in aqueous environment found for MnBePO_5 , KV_2PO_8 , SrV_2O_6 , and $\text{Mo}_2\text{P}_2\text{O}_{11}$ ($\langle\Delta G_{\text{pbx}}\rangle > 0.10$ eV atom $^{-1}$) positions them as of secondary priority for experimental testing when compared to the FePO_4 polymorphs. Finally, the remaining proposed materials, $\text{Cs}_2\text{Mo}_4\text{O}_{13}$, $\text{K}_3\text{Fe}_5(\text{PO}_4)_6$, $\text{CaFe}_3\text{P}_3\text{O}_{13}$, and $\text{SrFe}_3\text{P}_3\text{O}_{13}$, are mainly of interest as RAZIB cathodes due to their higher electrochemical stability ($\langle\Delta G_{\text{pbx}}\rangle < 0.10$ eV atom $^{-1}$), potentially granting them longer stable operation, despite their subpar E_{Zn} , Q_{w} , and W_{w} metrics.

The complete E_{Zn} profile for α - FePO_4 was then calculated to further probe its utilization as cathode for RAZIBs, with the results being shown in Figure 5a. To obtain the E_{Zn} curve for α - FePO_4 , discharged structures with different stoichiometries were created by randomly placing Zn atoms in the percolation paths identified within its structure for $d_{\text{perc}}^{\text{max}}(\delta_{\text{perc}} < 0.7$ Å). The fully discharged structure was considered to be $\text{Zn}_{0.5}\text{FePO}_4$ in order to capture a full one electron reduction for the Fe atoms from $\text{Fe}_{(\text{s})}^{3+}$ to $\text{Fe}_{(\text{s})}^{2+}$. As can be seen from the potential curve presented in Figure 5a, the E_{Zn} for α - FePO_4 decreases throughout the Zn^{2+} intercalation process from the initial potential of 1.34 V vs Zn/Zn^{2+} . The E_{Zn}

Table 3: Selected materials proposed for experimental testing based on the calculated Zn^{2+} (de)intercalation potential (E_{Zn}), average electrochemical decomposition energy ($\langle \Delta G_{pbx} \rangle$), theoretical gravimetric capacity (Q_w), and theoretical energy density (W_w).

Material	E_{Zn} (V vs Zn/Zn^{2+})	$\langle \Delta G_{pbx} \rangle$ (eV atom $^{-1}$)	Q_w (mA h g $^{-1}$)	W_w (W h kg $^{-1}$)
$MnBePO_5$ (mp-1197976)	1.67	0.20	153.2	256.5
α -FePO ₄ (mp-19109)	1.34	0.06	177.7	238.1
β -FePO ₄ (mp-19752)	1.32	0.06	177.7	234.6
KV ₂ PO ₈ (mp-557947)	1.30	0.11	178.7	231.8
SrV ₂ O ₆ (mp-19038)	1.29	0.13	187.8	242.8
Mo ₂ P ₂ O ₁₁ (mp-636950)	1.25	0.15	124.7	155.8
Cs ₂ Mo ₄ O ₁₃ (mp-1202511)	1.01	0.07	125.0	126.0
K ₃ Fe ₅ (PO ₄) ₆ (mp-566670)	0.89	0.05	138.7	123.0
CaFe ₃ P ₃ O ₁₃ (mp-560784)	0.87	0.05	158.1	138.0
SrFe ₃ P ₃ O ₁₃ (mp-557942)	0.86	0.04	144.6	124.3

discharge curve for α -FePO₄ captured by our calculations also matches the experimental potential curve reported for the discharge of other FePO₄ phases as RAZIB cathodes,^{75,87} which further highlights the potential of α -FePO₄ as a cathode material. The theoretical E_{Zn} curve for α -FePO₄ also predicts that the theoretical capacity of 177.7 mA h g $^{-1}$ can be achieved within the potential window for safe electrolyte operation ($E(\text{HER}) < E_{Zn} < E(\text{OER})$). However, it is important to note that the E_{Zn} calculated for the fully discharged material is very low ($E_{Zn}(Zn_{0.5}\text{FePO}_4) = 0.50$ V vs Zn/Zn^{2+}) and close to the potential for HER at the considered operation conditions ($E(\text{HER}) = 0.468$ V vs Zn/Zn^{2+} , pH = 5 and $[Zn^{2+}] = 1$ M), which limits the feasibility of achieving the full theoretical capacity during experimental battery operation. By calculating the complete E_{Zn} curve for α -FePO₄, the investigation of the cell volume variation due to the Zn^{2+} intercalation into the structure was also made possible. A cell volume reduction of approximately 4% was observed when comparing the calculated relaxed cell volumes between the fully charged (α -FePO₄) and discharged (α -Zn_{0.5}FePO₄) phases, which indicates that the favourable intercalation of Zn^{2+} into the structure causes a contraction of the atomic spacing.

The DOS and pDOS for α -FePO₄ was also calculated, alongside the crystal orbital Hamil-

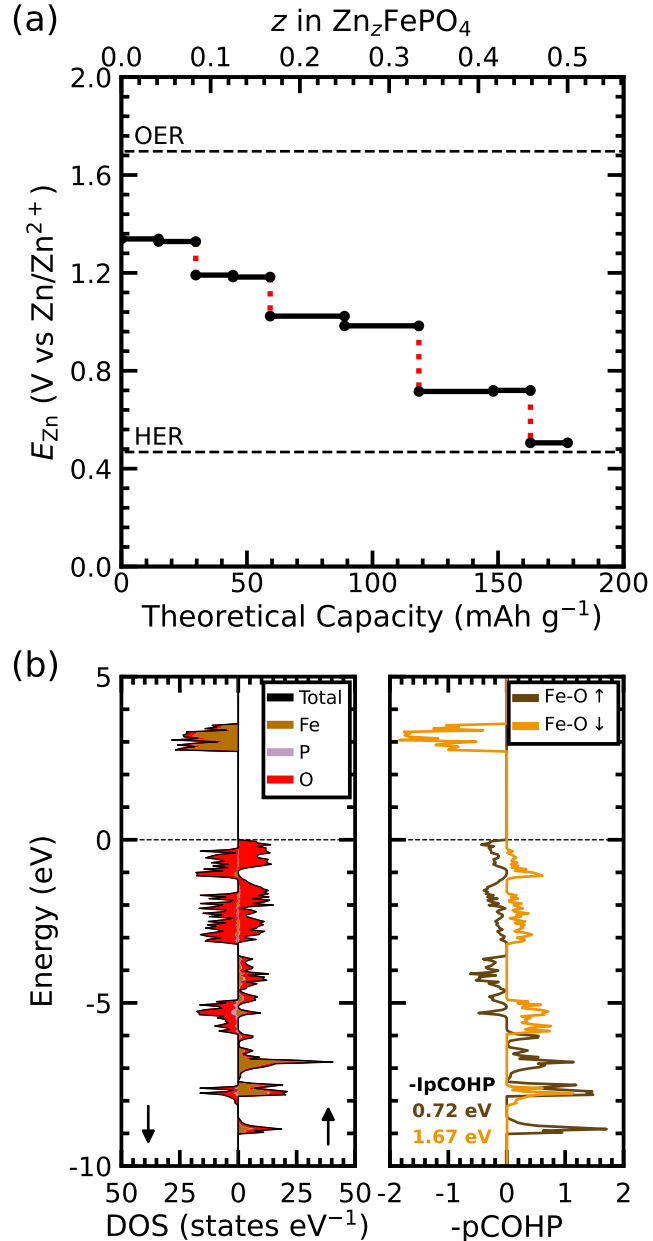


Figure 5: (a) Complete Zn²⁺ (de)intercalation potential (E_{Zn}) profile predicted for $\alpha\text{-FePO}_4$. The dashed black lines represent the HER and OER potential calculated at a pH = 5 and $[\text{Zn}^{2+}] = 1 \text{ M}$. (b) Density of states (DOS) and projected density of states (pDOS) results for $\alpha\text{-FePO}_4$ with the associated projected crystal orbital Hamilton population (pCOHP) analysis results for the Fe-O bond in the structure. Energy is shifted so the Fermi energy (E_F) is at 0 eV.

ton population (COHP) analysis for the Fe-O bonding in the structure (Fig. 5b), in order to understand the electronic structure of the proposed cathode material. Equivalent calculations were also performed for the *olivine* polymorph of FePO₄ to allow for a comparison to a previously investigated RAZIB cathode material,⁷⁵ with the results being presented in Figure S9. Overall, similar results were seen with respect to the pDOS results for both FePO₄ materials, with the valence states close to the E_F having a strong O character, and the lower energy conductive states being comprised of Fe orbitals in its majority. The main difference between the results for the two FePO₄ polymorphs was observed on the COHP analysis. The Fe-O bonds in α -FePO₄ were confirmed to be stronger covalent bonds than in *olivine*-FePO₄ for both spins, as the negative integrated projected crystal orbital Hamilton population (-IpCOHP) up to the E_F was greater in α -FePO₄ than in *olivine*-FePO₄ (see Figs. 5b and S9). The stronger covalency for the Fe-O bonds in α -FePO₄ captured by -IpCOHP indicates a higher stability of the Fe bonds in the material when compared to the same bonds in *olivine*-FePO₄, further supporting the proposal of α -FePO₄ as a RAZIB cathode material. It is important to note that Fe-O bonding complexes (tetrahedral coordination (FeO₄) in α -FePO₄ and octahedral coordination (FeO₆) in *olivine*-FePO₄) will undergo structural distortions and reduction of the transition metal oxidation state once the Zn²⁺ atoms intercalate in the structure, which may be harder to accommodate in α -FePO₄ due to the stronger Fe-O bonding present in the structure. However, the successful utilization of α -FePO₄ as a cathode material in LIB demonstrates the feasibility of ionic intercalation into its structure⁸⁸⁻⁹⁰ and further showcases the potential of α -FePO₄ as a next-generation RAZIB cathode material.

Conclusion

In this study, a comprehensive screening of previously synthesized oxides, chalcogenides, Prussian blue analogues (PBAs) and polyanions as novel rechargeable aqueous zinc-ion bat-

tery (RAZIB) cathodes was performed. The data from more than 2000 experimentally confirmed materials was retrieved from the Materials Project database, with their structural availability for Zn^{2+} migration, electrochemical stability in aqueous media and chemical feasibility for use as a cathode being evaluated. In total, 131 materials were identified through the screening process as having suitable structural, electrochemical and chemical characteristics for operation as a RAZIB cathode, for which the Zn^{2+} (de)intercalation potential (E_{Zn}) was then calculated. Analysis of the E_{Zn} results revealed that higher potentials were obtained for materials that had transition metals at higher oxidation state in its structure and were also able to accommodate the intercalating Zn^{2+} ion on a favourable coordination environment. The determination of a relationship between metal oxidation state and ion coordination to E_{Zn} presented in this study contributes to future exploration of cathode materials with high operation potentials for RAZIBs, as well as other battery chemistries. 10 previously unexplored materials ($MnBePO_5$, α - $FePO_4$, β - $FePO_4$, KV_2PO_8 , SrV_2O_6 , $Mo_2P_2O_{11}$, $Cs_2Mo_4O_{13}$, $K_3Fe_5(PO_4)_6$, $CaFe_3P_3O_{13}$, and $SrFe_3P_3O_{13}$) with leading metrics for RAZIB operation, such as high intercalation potential, electrochemical stability, theoretical gravimetric capacity, and energy density, were identified and were here proposed for experimental investigation as RAZIB cathodes for the first time. The methodology employed in this study for the discovery of novel RAZIB cathode materials can also be employed for the exploration of cathode materials for other battery chemistries, in special with aqueous electrolytes, positively contributing for the continuous implementation of rechargeable batteries in grid-scale energy storage applications. The results contained in this study present a clear guideline for future RAZIB cathode material development by identifying novel materials with high operation potential and stability in support of the commercialization efforts for RAZIBs.

Author Contributions

- **Caio Miranda Miliante:** Conceptualization, Methodology, Software, Validation, Formal analysis, Investigation, Data curation, Writing - Original Draft, Writing - Review & Editing, Visualization, and Project administration.
- **Brian D. Adams:** Writing - Review & Editing, and Funding acquisition.
- **Drew Higgins:** Resources, Writing - Review & Editing, Supervision, and Funding acquisition.
- **Oleg Rubel:** Conceptualization, Resources, Writing - Review & Editing, Supervision, Funding acquisition.

Acknowledgement

The authors gratefully acknowledge the financial support from Salient Energy Inc. and the Natural Sciences and Engineering Research Council of Canada (NSERC) Alliance Program. C.M.M. acknowledges the Digital Research Alliance of Canada and Compute Ontario for the computing resources utilized in this research. C.M.M thanks Prof. Xavier Rocquefelte (University of Rennes) for the discussion about the utilization of crystal orbital Hamilton population (COHP) for the analysis of the proposed materials.

Supporting Information Available

The supporting information for the paper includes figures for: the distribution of queried materials with respect to the class and transition metal centre; maximum percolation path distance (d_{perc}^{\max}) and average electrochemical decomposition energy ($\langle \Delta G_{\text{pbx}} \rangle$) results for all screened materials separated by material class; d_{perc}^{\max} and $\langle \Delta G_{\text{pbx}} \rangle$ results for chalcogenide materials colour-coded by chalcogenide centre (S, Se, and Te); percolation path

associated with d_{perc}^{\max} for Li_3VO_4 and $\text{Sr}_2\text{V}_2\text{O}_7$; distribution of material selected for Zn^{2+} (de)intercalation potential (E_{Zn}) calculation with respect to their class (oxide or polyanion) and transition metal centre; E_{Zn} results separated by transition metal centre and colour-coded by average metal centre oxidation state in the material; Zn^{2+} coordination environment in RbVPHO_6 , Rb_2MoO_4 , Li_3VO_4 , KV_2PO_8 , $\text{Cs}_2\text{Mo}_4\text{O}_{13}$, and BaV_2O_6 after relaxation; density of states (DOS), projected density of states (pDOS) and projected crystal orbital Hamilton population (pCOHP) results for *olivine*- FePO_4 .

The Python code developed for this study is available online, with the compiled data for all materials utilized for parameter screening available at a Zenodo repository.

References

- (1) Zhu, Z.; Jiang, T.; Ali, M.; Meng, Y.; Jin, Y.; Cui, Y.; Chen, W. Rechargeable batteries for grid scale energy storage. *Chem. Rev.* **2022**, *122*, 16610–16751.
- (2) Gallo, A.; Simões-Moreira, J. R.; Costa, H.; Santos, M. M.; Dos Santos, E. M. Energy storage in the energy transition context: a technology review. *Renew. Sustain. Energy Rev.* **2016**, *65*, 800–822.
- (3) Gourley, S. W.; Brown, R.; Adams, B. D.; Higgins, D. Zinc-ion batteries for stationary energy storage. *Joule* **2023**, *7*, 1415–1436.
- (4) Gupta, D.; Liu, S.; Zhang, R.; Guo, Z. Future Long Cycling Life Cathodes for Aqueous Zinc-Ion Batteries in Grid-Scale Energy Storage. *Adv. Energy Mater.* **2025**, *15*, 2500171.
- (5) Fan, Y.; Wang, Q.; Xie, Y.; Zhou, N.; Yang, Y.; Ding, Y.; Wei, Y.; Qu, G. Advances in aqueous zinc-ion battery systems: Cathode materials and chemistry. *Progress in Materials Science* **2025**, *149*, 101393.

(6) Li, G.; Sun, L.; Zhang, S.; Zhang, C.; Jin, H.; Davey, K.; Liang, G.; Liu, S.; Mao, J.; Guo, Z. Developing cathode materials for aqueous zinc ion batteries: challenges and practical prospects. *Adv. Funct. Mater.* **2024**, *34*, 2301291.

(7) Miliante, C.; Gourley, S.; Adams, B.; Higgins, D.; Rubel, O. Roadmap for the development of transition metal oxide cathodes for rechargeable zinc-ion batteries. *J. Phys. Chem. C* **2024**, *128*, 17261–17273.

(8) Zhang, Y.; Li, Y.; Yao, S.; Ali, N.; Kong, X.; Wang, J. High-performance organic electrodes for sustainable zinc-ion batteries: Advances, challenges and perspectives. *Energy Storage Mater.* **2024**, *103*, 103544.

(9) Cui, H.; Ma, L.; Huang, Z.; Chen, Z.; Zhi, C. Organic materials-based cathode for zinc ion battery. *SmartMat* **2022**, *3*, 565–581.

(10) Espinoza, A. I.; Baker, T. J.; Gourley, S. W.; Miliante, C. M.; Sanders, K. J.; Liu, Z.; Goward, G. R.; Rubel, O.; Adams, B. D.; Higgins, D. A tert-butyl functionalized quinone as active material for rechargeable aqueous zinc-ion batteries exhibiting high round-trip efficiency. *Future Batteries* **2025**, *100092*.

(11) Cui, J.; Guo, Z.; Yi, J.; Liu, X.; Wu, K.; Liang, P.; Li, Q.; Liu, Y.; Wang, Y.; Xia, Y.; others Organic cathode materials for rechargeable zinc batteries: mechanisms, challenges, and perspectives. *ChemSusChem* **2020**, *13*, 2160–2185.

(12) Baker, T. J.; Espinoza, A. I.; Gourley, S. W.; Adams, B. D.; Higgins, D. Stabilizing redox-active organic molecules via grafting to carbon for cathodes in aqueous rechargeable zinc-ion batteries. *J. Energy Storage* **2026**, *150*, 120312.

(13) Xu, C.; Li, B.; Du, H.; Kang, F. Energetic zinc ion chemistry: The rechargeable zinc ion battery. *Angew. Chem. Int. Ed.* **2011**, *51*, 933–935.

(14) Liao, Y.; Chen, H.-C.; Yang, C.; Liu, R.; Peng, Z.; Cao, H.; Wang, K. Unveiling performance evolution mechanisms of MnO_2 polymorphs for durable aqueous zinc-ion batteries. *Energy Storage Mater.* **2022**, *44*, 508–516.

(15) Rubel, O.; Tran, T. N. T.; Gourley, S.; Anand, S.; Bommel, A. V.; Adams, B. D.; Ivey, D. G.; Higgins, D. Electrochemical stability of ZnMn_2O_4 : understanding Zn-ion rechargeable battery capacity and degradation. *J. Phys. Chem. C* **2022**, *126*, 10957–10967.

(16) He, Y.; Tang, H.; Huang, Y.; Chen, K.; Wang, G.; Zheng, D.; Xu, W.; Wang, F.; Lu, X. Valence modulation and morphological engineering of MoO_3 as high-performance cathode for aqueous zinc ion batteries. *Electrochim. Acta* **2023**, *465*, 142988.

(17) Wu, J.; Meng, J.; Yang, Z.; Chen, H.; Rong, Y.; Deng, L.; Fu, Z. Energy storage mechanism and electrochemical performance of $\text{Cu}_2\text{O}/\text{rGO}$ as advanced cathode for aqueous zinc ion batteries. *J. Alloys Compd.* **2022**, *895*, 162653.

(18) Bin, D.; Du, Y.; Yang, B.; Lu, H.; Liu, Y.; Xia, Y. Progress of phosphate-based polyanion cathodes for aqueous rechargeable zinc batteries. *Adv. Funct. Mater.* **2023**, *33*, 2211765.

(19) Ou, L.; Ou, H.; Qin, M.; Liu, Z.; Fang, G.; Cao, X.; Liang, S. Recent progress on phosphate cathode materials for aqueous zinc-ion batteries. *ChemSusChem* **2022**, *15*, e202201184.

(20) Ni, Q.; Bai, Y.; Wu, F.; Wu, C. Polyanion-type electrode materials for sodium-ion batteries. *Adv. Sci.* **2017**, *4*, 1600275.

(21) Zampardi, G.; La Mantia, F. Prussian blue analogues as aqueous Zn-ion batteries electrodes: Current challenges and future perspectives. *Curr. Opin. Electrochem.* **2020**, *21*, 84–92.

(22) Liu, J.; Shen, Z.; Lu, C.-Z. Research progress of Prussian blue and its analogues for cathodes of aqueous zinc ion batteries. *J. Mater. Chem. A* **2024**, *12*, 2647–2672.

(23) Wang, L.; Li, S.; Wang, C.; Yao, S.; Chen, G.; Du, F. Recent advance and design strategies of chalcogenides for high-performance aqueous zinc-ion batteries. *J. Phys. D: Appl. Phys.* **2024**, *57*, 253001.

(24) Zhou, T.; Zhu, L.; Xie, L.; Han, Q.; Yang, X.; Chen, L.; Wang, G.; Cao, X. Cathode materials for aqueous zinc-ion batteries: a mini review. *J. Colloid Interface Sci.* **2022**, *605*, 828–850.

(25) Park, S.; Park, S.; Park, Y.; Alfaruqi, M. H.; Hwang, J.-Y.; Kim, J. A new material discovery platform of stable layered oxide cathodes for K-ion batteries. *Energy Environ. Sci.* **2021**, *14*, 5864–5874.

(26) Mueller, T.; Hautier, G.; Jain, A.; Ceder, G. Evaluation of tavorite-structured cathode materials for lithium-ion batteries using high-throughput computing. *Chem. Mater.* **2011**, *23*, 3854–3862.

(27) Hautier, G.; Jain, A.; Chen, H.; Moore, C.; Ong, S. P.; Ceder, G. Novel mixed polyanions lithium-ion battery cathode materials predicted by high-throughput ab initio computations. *J. Mater. Chem.* **2011**, *21*, 17147–17153.

(28) Kim, J.; Sari, D.; Chen, Q.; Ceder, G.; Persson, K. A. Evaluating Material Design Principles for Calcium-Ion Mobility in Intercalation Cathodes. *Chem. Mater.* **2024**, *37*, 507–519.

(29) Zhu, B.; Lu, Z.; Pickard, C. J.; Scanlon, D. O. Accelerating cathode material discovery through ab initio random structure searching. *APL Mater.* **2021**, *9*.

(30) Chen, H.; Hautier, G.; Jain, A.; Moore, C.; Kang, B.; Doe, R.; Wu, L.; Zhu, Y.;

Tang, Y.; Ceder, G. Carbonophosphates: a new family of cathode materials for Li-ion batteries identified computationally. *Chem. Mater.* **2012**, *24*, 2009–2016.

(31) Nishijima, M.; Ootani, T.; Kamimura, Y.; Sueki, T.; Esaki, S.; Murai, S.; Fujita, K.; Tanaka, K.; Ohira, K.; Koyama, Y.; others Accelerated discovery of cathode materials with prolonged cycle life for lithium-ion battery. *Nat. Commun.* **2014**, *5*, 4553.

(32) Zhou, L.; Yao, A. M.; Wu, Y.; Hu, Z.; Huang, Y.; Hong, Z. Machine learning assisted prediction of cathode materials for Zn-ion batteries. *Adv. Theory Simul.* **2021**, *4*, 2100196.

(33) Cai, J.; Wang, Z.; Wu, S.; Han, Y.; Li, J. A machine learning shortcut for screening the spinel structures of Mg/Zn ion battery cathodes with a high conductivity and rapid ion kinetics. *Energy Storage Mater.* **2021**, *42*, 277–285.

(34) Wudil, Y. S.; Gondal, M. A.; Al-Osta, M. A. High-throughput screening of 6858 compounds for zinc-ion battery cathodes via hybrid machine learning optimization. *ACS Appl. Mater. Interfaces* **2025**, *17*, 10603–10616.

(35) Jain, A.; Ong, S. P.; Hautier, G.; Chen, W.; Richards, W. D.; Dacek, S.; Cholia, S.; Gunter, D.; Skinner, D.; Ceder, G.; others Commentary: The Materials Project: A materials genome approach to accelerating materials innovation. *APL Mater.* **2013**, *1*, 011002.

(36) Ong, S. P.; Cholia, S.; Jain, A.; Brafman, M.; Gunter, D.; Ceder, G.; Persson, K. A. The Materials Application Programming Interface (API): A simple, flexible and efficient API for materials data based on REpresentational State Transfer (REST) principles. *Comput. Mater. Sci.* **2015**, *97*, 209–215.

(37) Wu, D.; Housel, L. M.; Kim, S. J.; Sadique, N.; Quilty, C. D.; Wu, L.; Tappero, R.; Nicholas, S. L.; Ehrlich, S.; Zhu, Y.; others Quantitative temporally and spatially

resolved X-ray fluorescence microprobe characterization of the manganese dissolution-deposition mechanism in aqueous Zn/ α -MnO₂ batteries. *Energy Environ. Sci.* **2020**, *13*, 4322–4333.

(38) Bischoff, C. F.; Fitz, O. S.; Burns, J.; Bauer, M.; Gentscher, H.; Birke, K. P.; Henning, H.-M.; Biro, D. Revealing the local pH value changes of acidic aqueous zinc ion batteries with a manganese dioxide electrode during cycling. *J. Electrochem. Soc.* **2020**, *167*, 020545.

(39) Persson, K. A.; Waldwick, B.; Lazic, P.; Ceder, G. Prediction of solid-aqueous equilibria: Scheme to combine first-principles calculations of solids with experimental aqueous states. *Phys. Rev. B* **2012**, *85*, 235438.

(40) Singh, A. K.; Zhou, L.; Shinde, A.; Suram, S. K.; Montoya, J. H.; Winston, D.; Gregoire, J. M.; Persson, K. A. Electrochemical stability of metastable materials. *Chem. Mater.* **2017**, *29*, 10159–10167.

(41) Patel, A. M.; Nørskov, J. K.; Persson, K. A.; Montoya, J. H. Efficient Pourbaix diagrams of many-element compounds. *Phys. Chem. Chem. Phys.* **2019**, *21*, 25323–25327.

(42) Rodríguez-Pérez, I. A.; Chang, H. J.; Fayette, M.; Sivakumar, B. M.; Choi, D.; Li, X.; Reed, D. Mechanistic investigation of redox processes in Zn–MnO₂ battery in mild aqueous electrolytes. *J. Mater. Chem. A* **2021**, *9*, 20766–20775.

(43) Batatia, I.; Kovacs, D. P.; Simm, G.; Ortner, C.; Csányi, G. MACE: Higher order equivariant message passing neural networks for fast and accurate force fields. *Adv. Neural Inf. Process. Syst.* **2022**, *35*, 11423–11436.

(44) Batatia, I.; Benner, P.; Chiang, Y.; Elena, A. M.; Kovács, D. P.; Riebesell, J.; Advincula, X. R.; Asta, M.; Avaylon, M.; Baldwin, W. J.; others A foundation model for atomistic materials chemistry. *arXiv preprint arXiv:2401.00096* **2023**,

(45) Melchionna, S.; Ciccotti, G.; Lee Holian, B. Hoover NPT dynamics for systems varying in shape and size. *Mol. Phys.* **1993**, *78*, 533–544.

(46) Melchionna, S. Constrained systems and statistical distribution. *Phys. Rev. E* **2000**, *61*, 6165.

(47) Larsen, A. H.; Mortensen, J. J.; Blomqvist, J.; Castelli, I. E.; Christensen, R.; Dułak, M.; Friis, J.; Groves, M. N.; Hammer, B.; Hargus, C.; others The atomic simulation environment—a Python library for working with atoms. *J. Phys. Condens. Matter* **2017**, *29*, 273002.

(48) Dronskowski, R.; Bloechl, P. E. Crystal orbital Hamilton populations (COHP): energy-resolved visualization of chemical bonding in solids based on density-functional calculations. *J. Phys. Chem.* **1993**, *97*, 8617–8624.

(49) Deringer, V. L.; Tchougréeff, A. L.; Dronskowski, R. Crystal orbital Hamilton population (COHP) analysis as projected from plane-wave basis sets. *J. Phys. Chem.* **2011**, *115*, 5461–5466.

(50) Maintz, S.; Deringer, V. L.; Tchougréeff, A. L.; Dronskowski, R. Analytic projection from plane-wave and PAW wavefunctions and application to chemical-bonding analysis in solids. *J. Comput. Chem.* **2013**, *34*, 2557–2567.

(51) Maintz, S.; Deringer, V. L.; Tchougréeff, A. L.; Dronskowski, R. LOBSTER: a tool to extract chemical bonding from plane-wave based DFT. 2016.

(52) Kresse, G.; Joubert, D. From ultrasoft pseudopotentials to the projector augmented-wave method. *Phys. Rev. B* **1999**, *59*, 1758–1775.

(53) Perdew, J. P.; Burke, K.; Ernzerhof, M. Generalized gradient approximation made simple. *Phys. Rev. Lett.* **1996**, *77*, 3865–3868.

(54) Kresse, G.; Hafner, J. Ab initio molecular dynamics for liquid metals. *Phys. Rev. B* **1993**, *47*, 558.

(55) Kresse, G.; Furthmüller, J. Efficiency of ab-initio total energy calculations for metals and semiconductors using a plane-wave basis set. *Comp. Mater. Sci.* **1996**, *6*, 15–50.

(56) Kresse, G.; Furthmüller, J. Efficient iterative schemes for ab initio total-energy calculations using a plane-wave basis set. *Phys. Rev. B* **1996**, *54*, 11169–11186.

(57) Grimme, S.; Antony, J.; Ehrlich, S.; Krieg, H. A consistent and accurate ab initio parametrization of density functional dispersion correction (DFT-D) for the 94 elements H–Pu. *J. Chem. Phys.* **2010**, *132*, 154104.

(58) Grimme, S.; Ehrlich, S.; Goerigk, L. Effect of the damping function in dispersion corrected density functional theory. *J. Comput. Chem.* **2011**, *32*, 1456–1465.

(59) Becke, A. D.; Johnson, E. R. A density-functional model of the dispersion interaction. *J. Chem. Phys.* **2005**, *123*.

(60) Johnson, E. R.; Becke, A. D. A post-Hartree–Fock model of intermolecular interactions. *J. Chem. Phys.* **2005**, *123*.

(61) Johnson, E. R.; Becke, A. D. A post-Hartree-Fock model of intermolecular interactions: Inclusion of higher-order corrections. *J. Chem. Phys.* **2006**, *124*.

(62) Jain, A.; Hautier, G.; Ong, S. P.; Moore, C. J.; Fischer, C. C.; Persson, K. A.; Ceder, G. Formation enthalpies by mixing GGA and GGA + U calculations. *Phys. Rev. B* **2011**, *84*, 045115.

(63) Dudarev, S. L.; Botton, G. A.; Savrasov, S. Y.; Humphreys, C. J.; Sutton, A. P. Electron-energy-loss spectra and the structural stability of nickel oxide: An LSDA+U study. *Phys. Rev. B* **1998**, *57*, 1505–1509.

(64) Pourbaix, M. *Atlas of electrochemical equilibria in aqueous solutions*, 2nd ed.; National Association of Corrosion Engineers, 1974.

(65) Ref. 64, chap. IV, sec. 19.2.

(66) Ref. 64, chap. IV, sec. 19.4.

(67) Ref. 64, chap. IV, sec. 19.3.

(68) Liu, Y.; Wu, X. Recent advances of transition metal chalcogenides as cathode materials for aqueous zinc-ion batteries. *Nanomaterials* **2022**, *12*, 3298.

(69) Ref. 64, chap. IV, sec. 17.1.

(70) Ref. 64, chap. IV, sec. 18.1.

(71) Zhao, S.; Wang, B.; Zhang, Z.; Zhang, X.; He, S.; Yu, H. First-principles computational insights into lithium battery cathode materials. *Electrochem. Energy Rev.* **2022**, *5*, 1–31.

(72) Rong, Z.; Kitchaev, D.; Canepa, P.; Huang, W.; Ceder, G. An efficient algorithm for finding the minimum energy path for cation migration in ionic materials. *J. Chem. Phys.* **2016**, *145*.

(73) He, P.; Yan, M.; Liao, X.; Luo, Y.; Mai, L.; Nan, C.-W. Reversible V^{3+}/V^{5+} double redox in lithium vanadium oxide cathode for zinc storage. *Energy Storage Mater.* **2020**, *29*, 113–120.

(74) Wu, M.; Shi, C.; Yang, J.; Zong, Y.; Chen, Y.; Ren, Z.; Zhao, Y.; Li, Z.; Zhang, W.; Wang, L.; others The LiV_3O_8 Superlattice Cathode with Optimized Zinc Ion Insertion Chemistry for High Mass-Loading Aqueous Zinc-Ion Batteries. *Adv. Mater.* **2024**, *36*, 2310434.

(75) Shimizu, M.; Tsuchikane, K.; Inoue, J.; Arai, S. Selective Zn/Na Ions Insertion into FePO₄ Positive Electrode Tuned by Counter Anions in Aqueous Zn-Based Rechargeable Batteries. *ChemElectroChem* **2024**, *11*, e202300540.

(76) Zhao, D.; Pu, X.; Tang, S.; Ding, M.; Zeng, Y.; Cao, Y.; Chen, Z. δ-VOPO₄ as a high-voltage cathode material for aqueous zinc-ion batteries. *Chem. Sci.* **2023**, *14*, 8206–8213.

(77) Xiao, H.; Du, X.; Li, R.; Jin, H.; Xie, L.; Han, Q.; Qiu, X.; Yang, X.; Zhu, L.; Cao, X. Polyoxovanadate Li₇[V₁₅O₃₆(CO₃)] and its derivative γ-LiV₂O₅ as superior performance cathode materials for aqueous zinc-ion batteries. *Chem. Eng. J.* **2024**, *489*, 151312.

(78) Lu, J.; Du, H.; Liu, H.; Cao, N.; Li, Z.; Cao, B. In situ constructing heterogeneous Mn(VO₃)₂/NaVO₃ nanoribbons as high-performance cathodes for aqueous zinc-ion batteries. *J. Alloys Compd.* **2024**, *975*, 172934.

(79) Goodenough, J. B.; Kim, Y. Challenges for rechargeable Li batteries. *Chem. Mater.* **2010**, *22*, 587–603.

(80) Padhi, A. K. Mapping redox energies of electrode materials for lithium batteries. Ph.D. thesis, The University of Texas at Austin, 1997.

(81) Barak, P.; Helmke, P. A. In *Zinc in Soils and Plants: Proceedings of the International Symposium on ‘Zinc in Soils and Plants’ held at The University of Western Australia, 27–28 September, 1993*; Robson, A. D., Ed.; Springer Netherlands: Dordrecht, 1993; Chapter 1, pp 1–13.

(82) Neumann, H. Notes on the mineralogy and geochemistry of zinc. *Mineral. Mag. J. Mineral. Soc.* **1949**, *28*, 575–581.

(83) Brehler, B. In *Elements Cr (24) to Br (35): Zinc - Crystal Chemistry*; Wedepohl, K. H.,

Correns, C. W., Shaw, D. M., Turekian, K. K., Zemann, J., Eds.; Handbook of Geochemistry:II-3; Springer, 1969; Vol. 1; Chapter 30-A.

(84) Jean, Y. *Molecular orbitals of transition metal complexes*; OUP Oxford, 2005; Chapter 2.

(85) Tang, B.; Zhou, J.; Fang, G.; Liu, F.; Zhu, C.; Wang, C.; Pan, A.; Liang, S. Engineering the interplanar spacing of ammonium vanadates as a high-performance aqueous zinc-ion battery cathode. *J. Mater. Chem. A* **2019**, *7*, 940–945.

(86) Dai, S.; Yang, C.; Huang, X.; Wang, Y.; Zeng, L. Recent Advances and Perspectives of Tunnel-Structured Nanomaterials for Zn-Ion Batteries. *Adv. Eng. Mater.* **2025**, e05291.

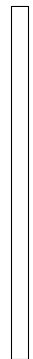
(87) Mathew, V.; Kim, S.; Kang, J.; Gim, J.; Song, J.; Baboo, J. P.; Park, W.; Ahn, D.; Han, J.; Gu, L.; others Amorphous iron phosphate: potential host for various charge carrier ions. *NPG Asia Mater* **2014**, *6*, e138–e138.

(88) Croce, F.; D'Epifanio, A.; Reale, P.; Settimi, L.; Scrosati, B. Ruthenium oxide-added quartz iron phosphate as a new intercalation electrode in rechargeable lithium cells. *J. Electrochem. Soc* **2003**, *150*, A576.

(89) Zhang, S.; Zhang, J.; Xu, S.; Yuan, X.; He, B. Li ion diffusivity and electrochemical properties of FePO_4 nanoparticles acted directly as cathode materials in lithium ion rechargeable batteries. *Electrochim. Acta* **2013**, *88*, 287–293.

(90) Song, Y.; Yang, S.; Zavalij, P. Y.; Whittingham, M. S. Temperature-dependent properties of FePO_4 cathode materials. *Mater. Res. Bull.* **2002**, *37*, 1249–1257.

TOC Graphic



Supporting Information:

Computational discovery of cathode materials for rechargeable aqueous zinc-ion batteries

Caio Miranda Miliante,^{*,†} Brian D. Adams,[‡] Drew Higgins,[¶] and Oleg Rubel[†]

[†]*Department of Materials Science and Engineering, McMaster University, 1280 Main Street West, Hamilton, Ontario L8S 4L8, Canada*

[‡]*Salient Energy Inc., Dartmouth, Nova Scotia B3B 1C4, Canada*

[¶]*Department of Chemical Engineering, McMaster University, 1280 Main Street West, Hamilton, Ontario L8S 4L8, Canada*

E-mail: miliantc@mcmaster.ca

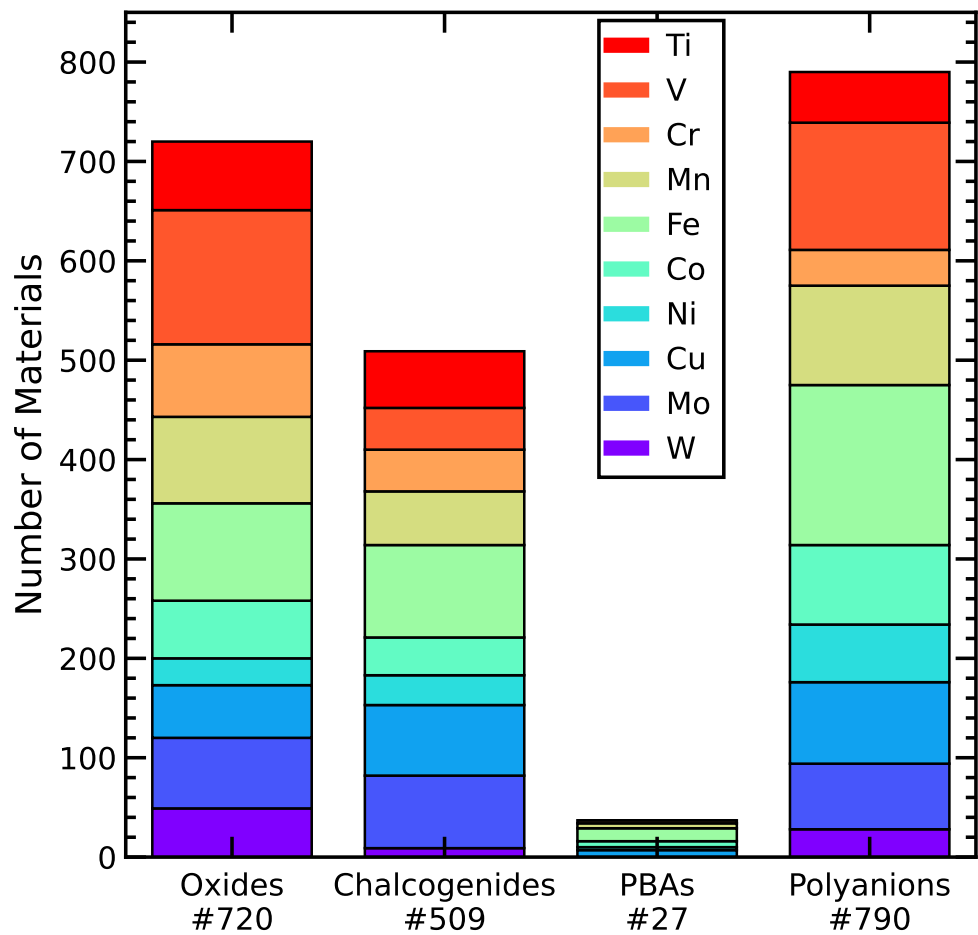


Figure S1: Distribution of queried materials from the database for each investigated material class colour-coded by transition metal centre.

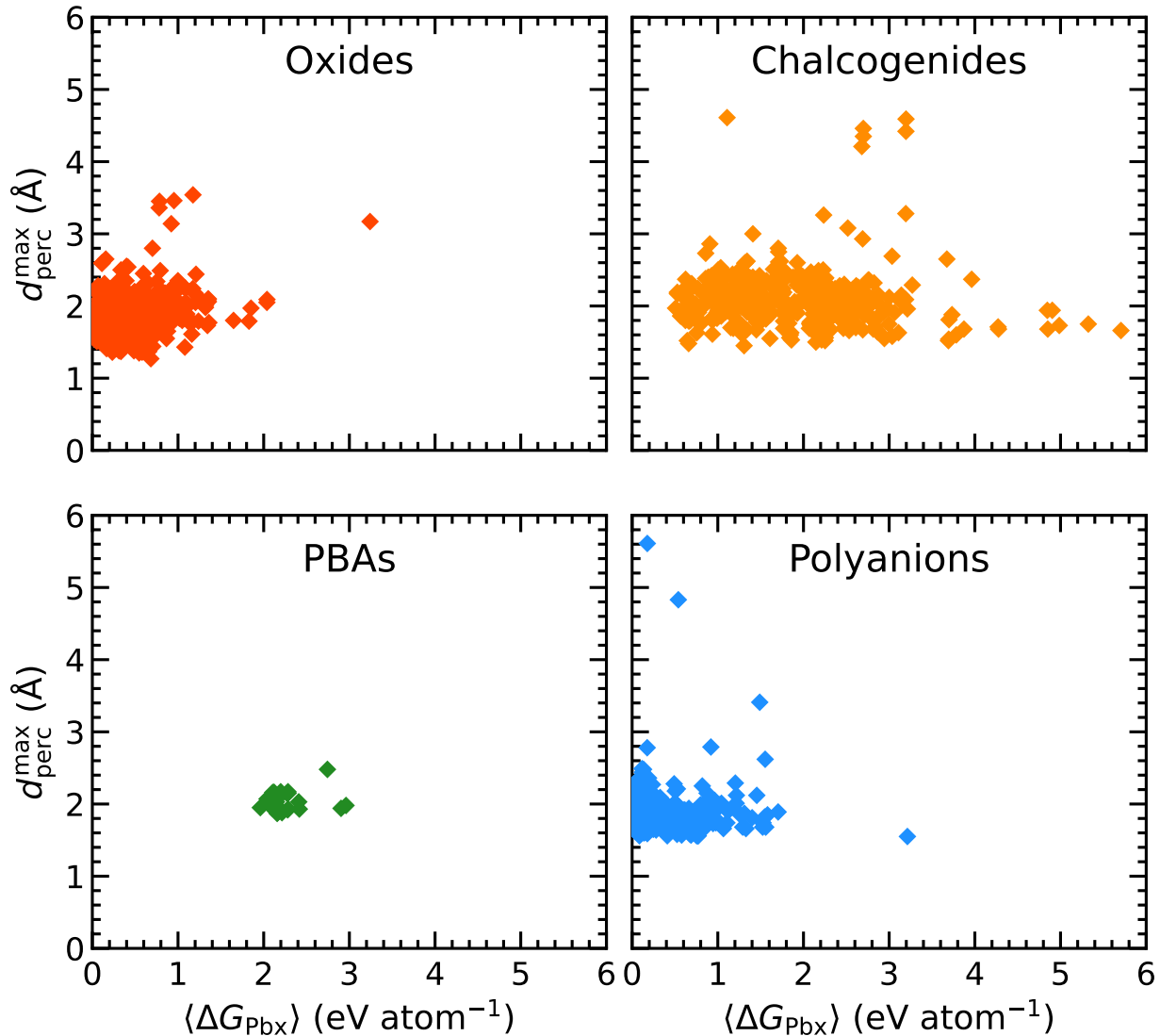


Figure S2: Maximum percolation path distance (d_{perc}^{\max}) and average electrochemical decomposition energy ($\langle \Delta G_{\text{Pbx}} \rangle$) results for all screened materials per material class.

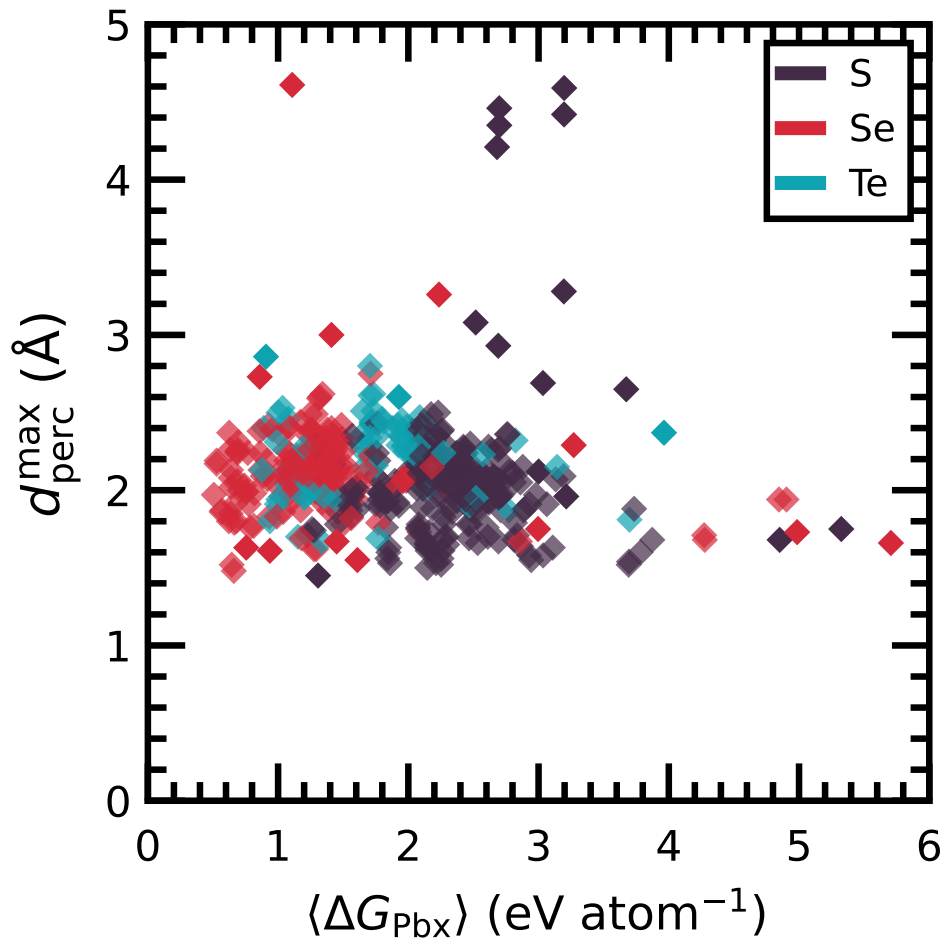


Figure S3: Maximum percolation path distance (d_{perc}^{\max}) and average electrochemical decomposition energy ($\langle \Delta G_{\text{Pbx}} \rangle$) for all materials indexed as a chalcogenide with respect to the chalcogenide atom present in the material.

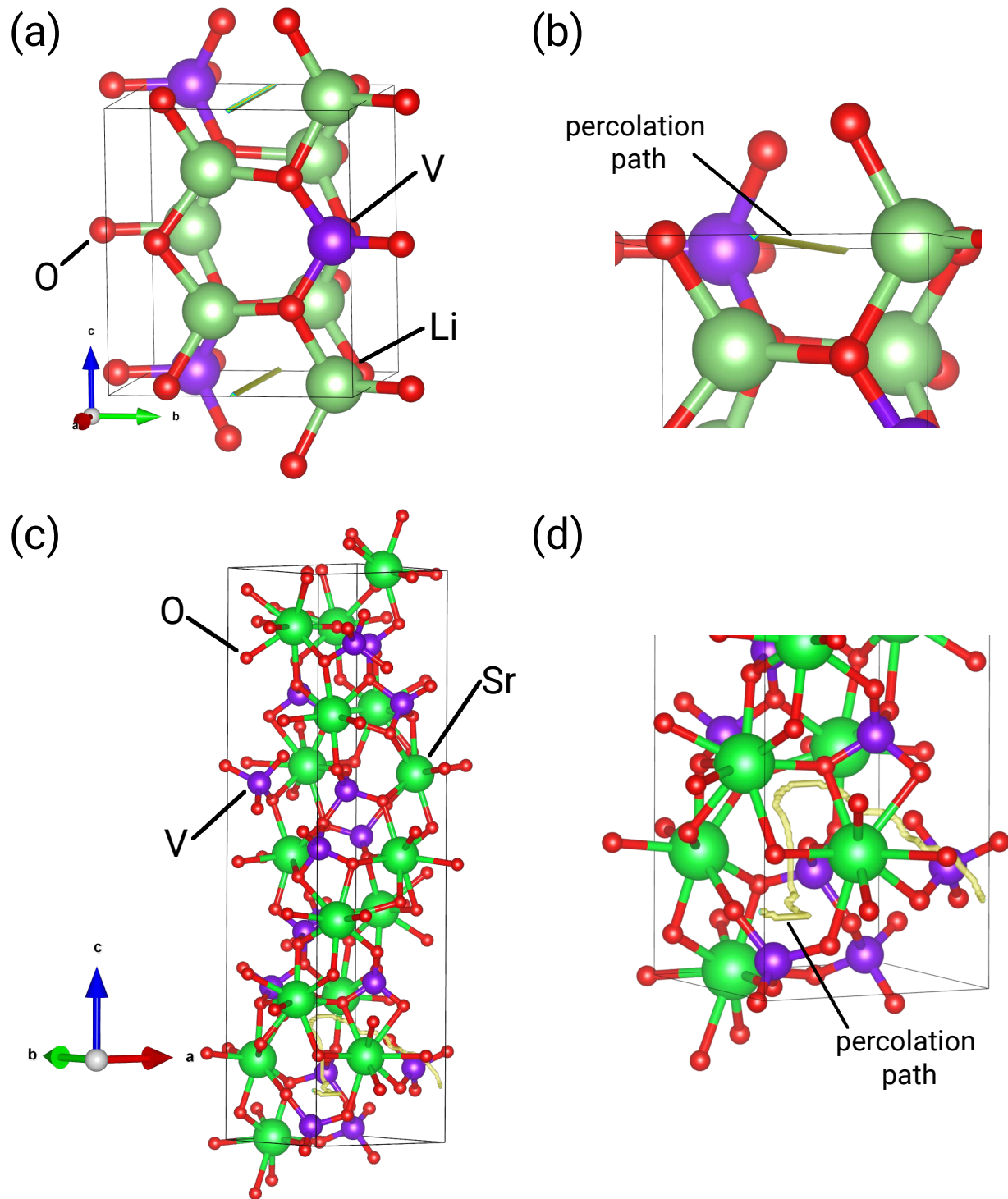


Figure S4: Percolation path associated with a maximum percolation path distance ($d_{\text{perc}}^{\text{max}}$) of 1.75 Å for (a,b) Li_3VO_4 (mp-19219) ($\delta_{\text{perc}} = 0.00$ Å) and (c,d) $\text{Sr}_2\text{V}_2\text{O}_7$ (mp-19660) ($\delta_{\text{perc}} = 4.74$ Å).

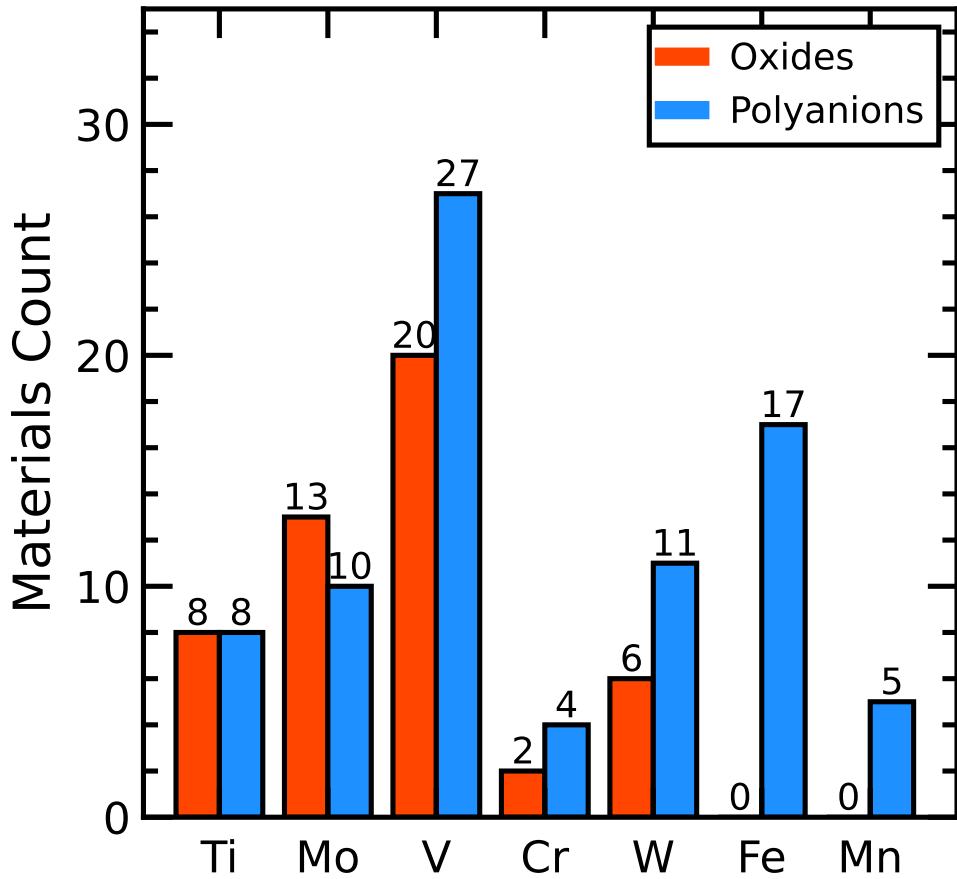


Figure S5: Materials selected for Zn^{2+} (de)intercalation potential (E_{Zn}) calculation separated by transition metal centre present in the structure.

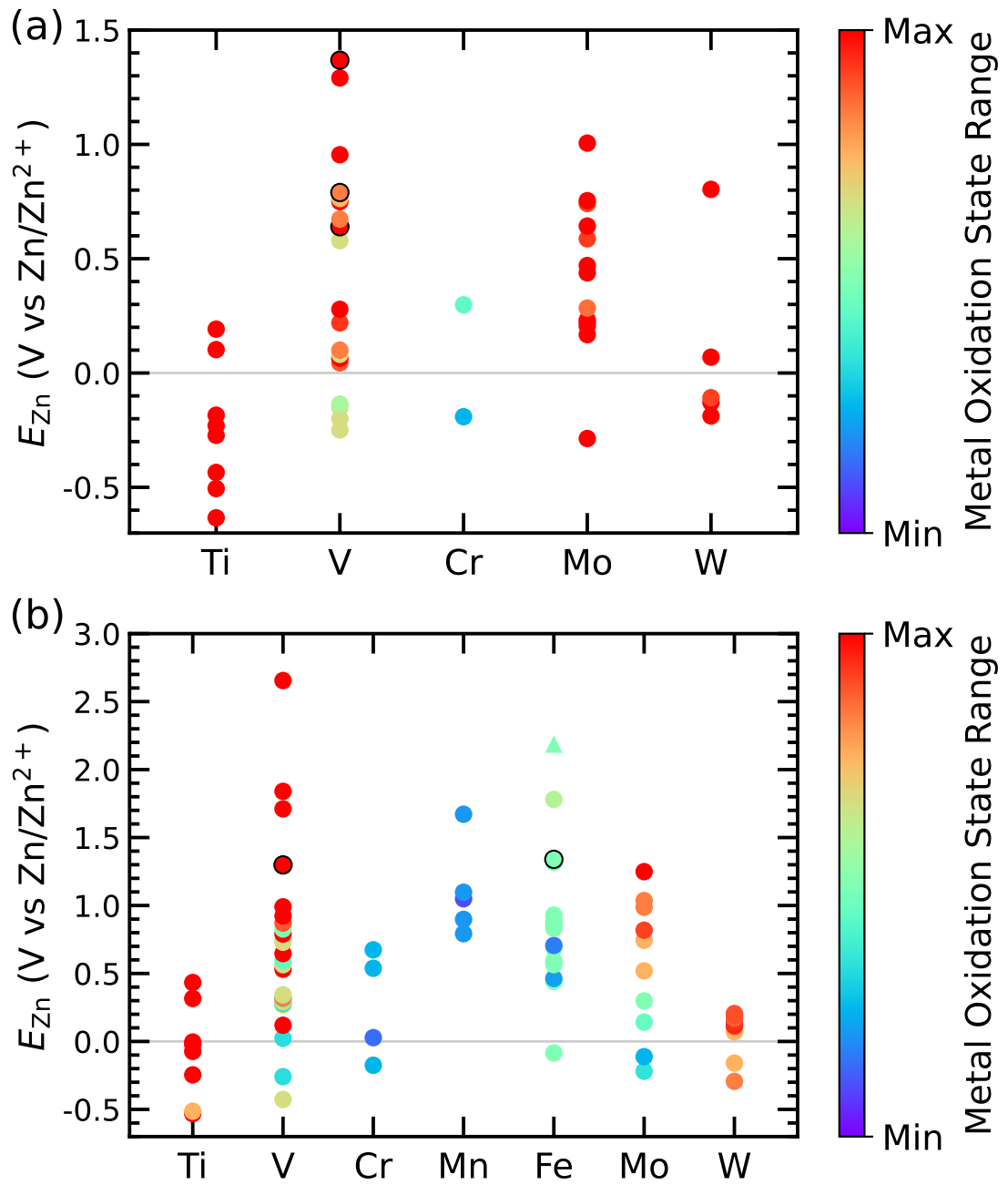


Figure S6: Zn^{2+} (de)intercalation potential (E_{Zn}) results per transition metal centre for (a) oxides and (b) polyanions colour-coded with respect to the lowest and highest experimentally confirmed oxidation state for each transition metal centre.

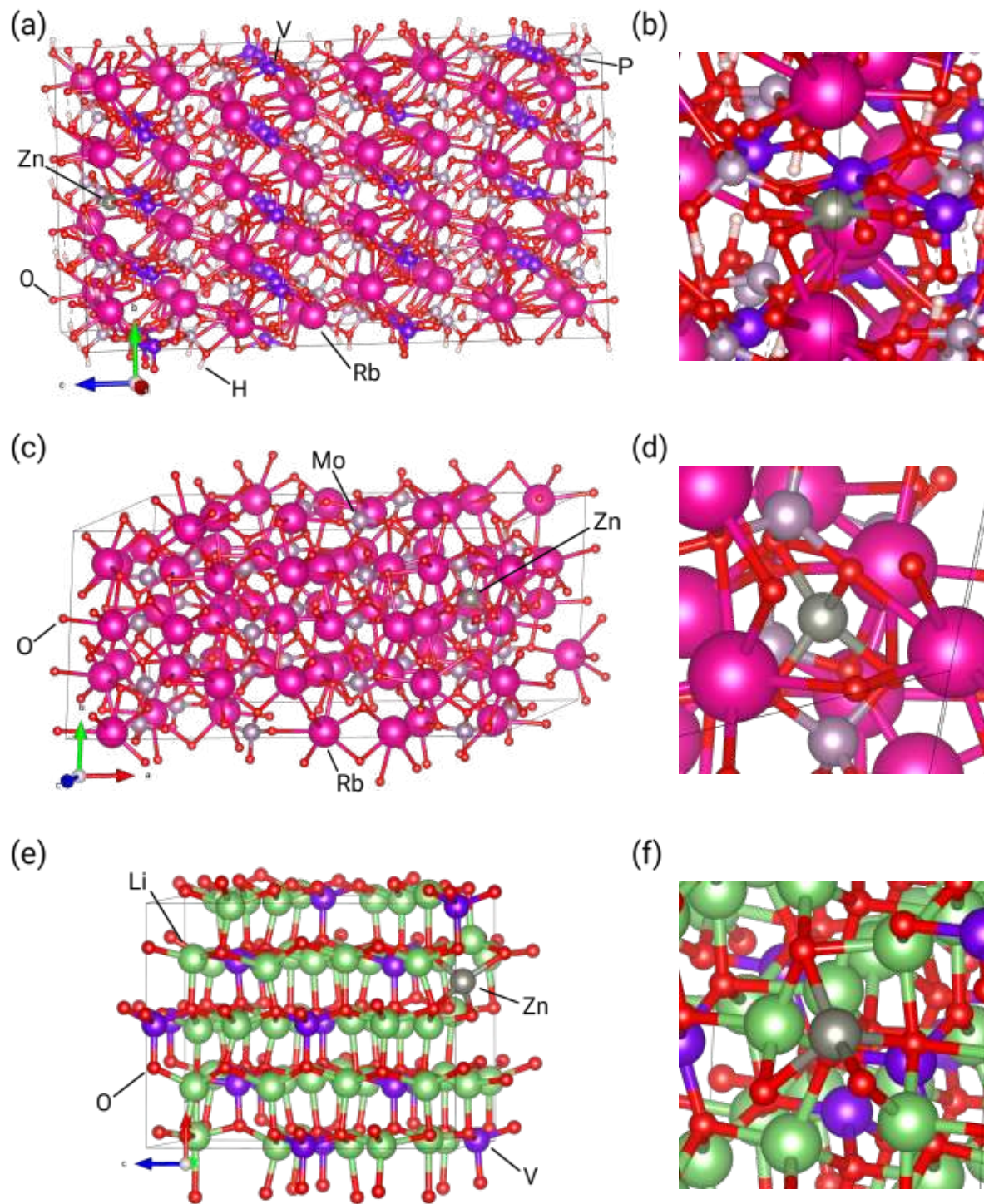


Figure S7: Relaxed crystal structure and associated Zn^{2+} coordination environment in (a,b) RbVPHO_6 (mp-1201601), (c,d) Rb_2MoO_4 (mp-19212), and (e,f) Li_3VO_4 (mp-19219).

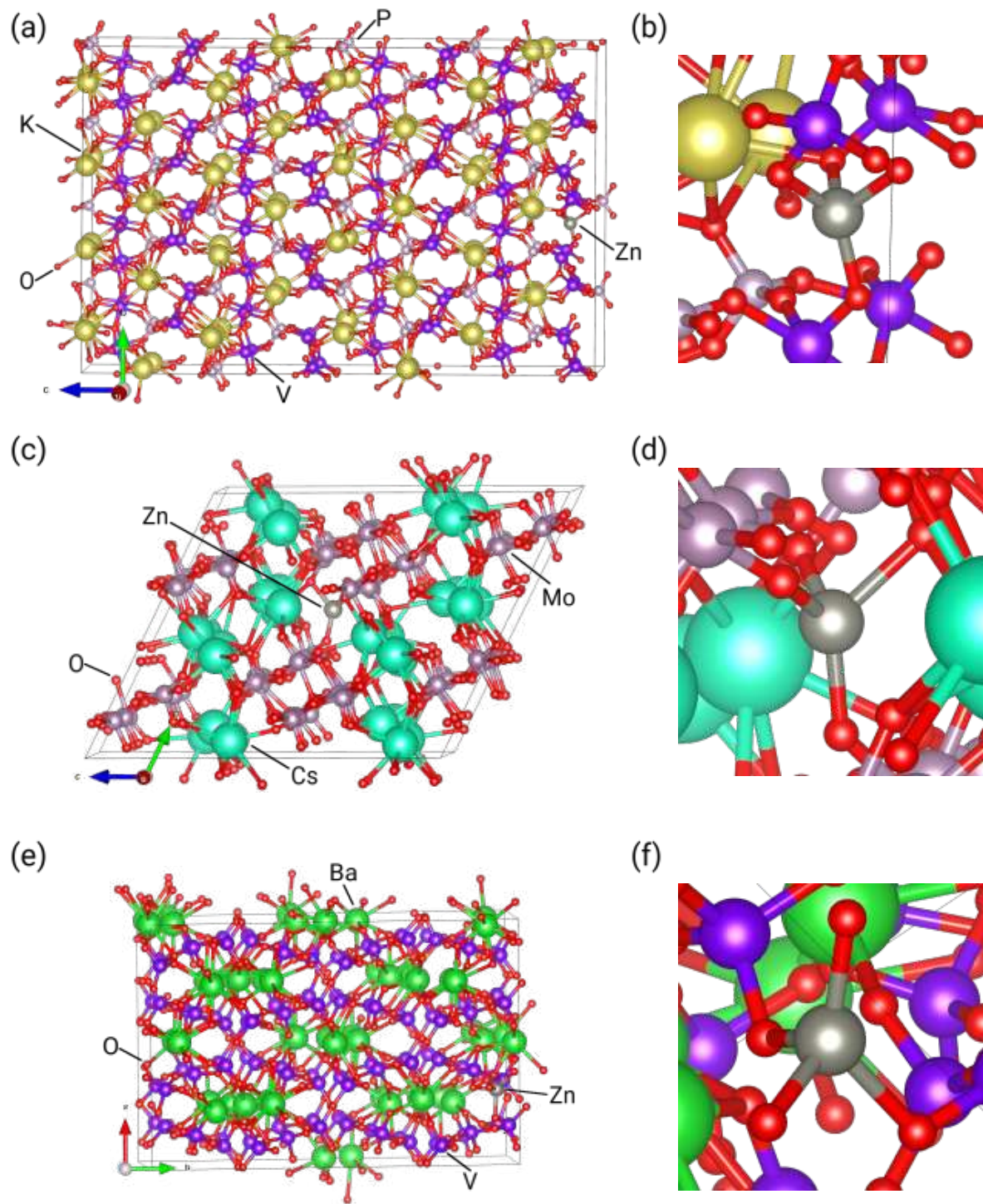


Figure S8: Relaxed crystal structure and associated Zn²⁺ coordination environment in (a,b) KV₂PO₈ (mp-557947), (c,d) Cs₂Mo₄O₁₃ (mp-1202511), and (e,f) BaV₂O₆ (mp-18929).

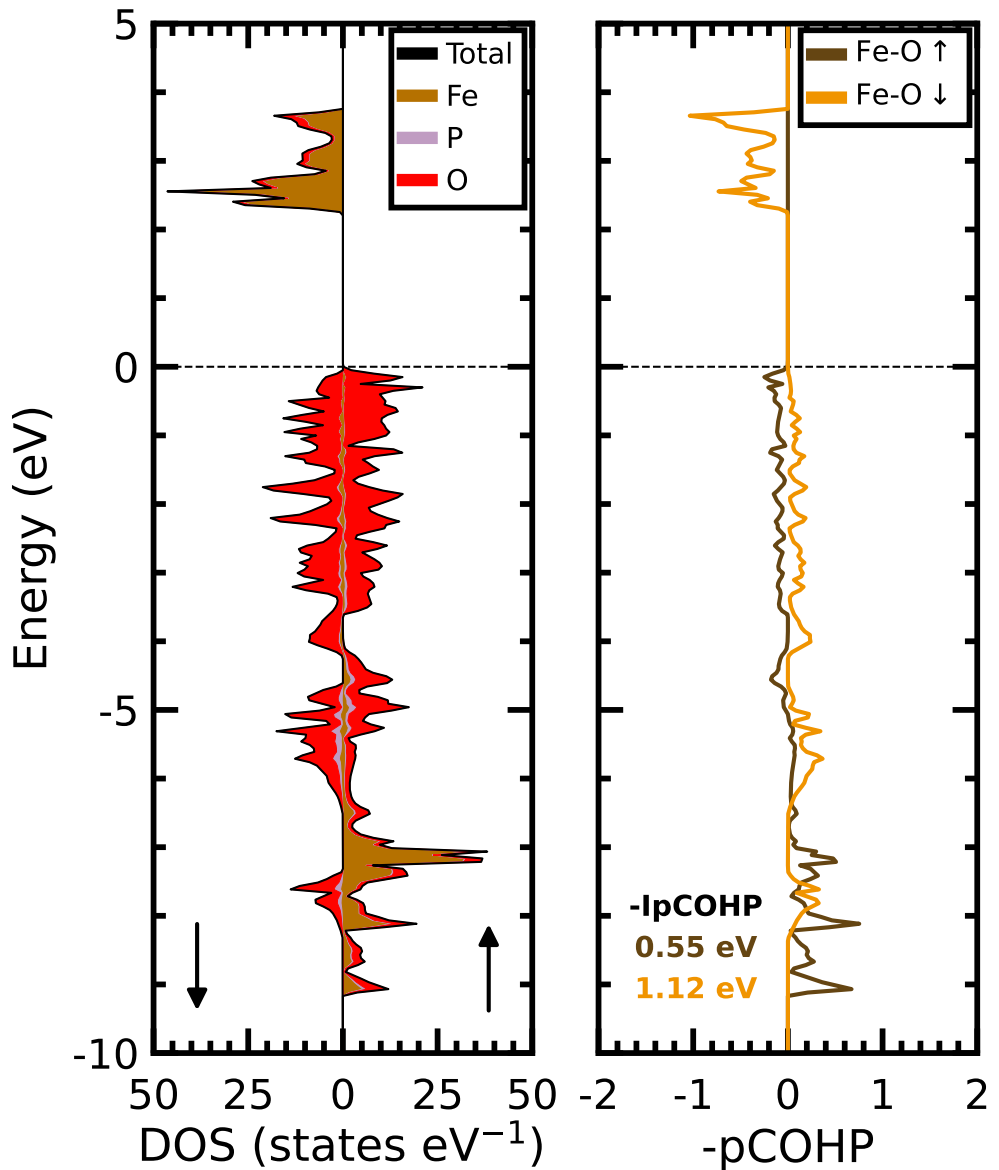


Figure S9: Density of states (DOS) and projected density of states (pDOS) results for olivine-FePO₄ (mp-20361), with the associated projected crystal orbital Hamilton population (pCOHP) analysis results for the Fe-O bond in the structure. Energy is shifted so the Fermi energy (E_F) is at 0 eV